Technical Developments to Enable Electrical Impedance Tomography (EIT) Measurement of Blood Flow to Monitor Cardiac Output:

Key Engineering Contributions

by

Helga Ross, BEng, Carleton University

A thesis submitted to

The Faculty of Graduate and Postdoctoral Affairs

In partial fulfilment of the requirements for the degree of

Master of Applied Science in Biomedical Engineering

Ottawa-Carleton Institute for Biomedical Engineering

Department of Systems and Computer Engineering

Carleton University

Ottawa, Ontario, Canada

September 2010

The undersigned hereby recommend to

the Faculty of Graduate and Postdoctoral Affairs

acceptance of the thesis

Technical Developments to Enable Electrical

Impedance Tomography (EIT) Measurement of

Blood Flow to Monitor Cardiac Output:

Key Engineering Contributions

Submitted by

Helga Ross, BEng, Carleton University

in partial fulfilment of the requirements

for the degree of Master of Applied Science in Biomedical Engineering

―――――――――――

Dr. Andy Adler, Thesis Supervisor

―――――――――――

Chair, Department of Systems and Computer Engineering

Dr. Howard Schwartz

Carleton University

September 2010

Abstract

The goal of this thesis is to develop a collection of Electrical Impedance Tomography (EIT) techniques to allow for bedside monitoring of cardiac output and other parameters of heart function such as left ventricle ejection ratio (LVER). EIT is an experimental imaging technique where changes inside the body can be imaged using a set of electrodes on the surface. The safe (non-ionising) and portable nature of this imaging system make it ideal for monitoring purposes. Though, laking in spatial resolution, EIT boasts a high temporal resolution which makes it a good candidate for cardiac monitoring. A strong need for monitoring cardiac parameters exists in diagnosis of Coronary Artery Disease (CAD). Recent cardiac EIT studies have shown promise in measuring cardiac output. Therefore, an EIT protocol was designed using some of the existing techniques. This EIT protocol was designed to fit into the existing University of Ottawa Heart Institute (UOHI) Computed Tomography (CT) protocol. A hardware setup was designed for EIT data acquisition and a software tool set was designed to extract the cardiac information from the EIT data. This software toolset includes a proposed novel temporal ensemble averaging technique. The proposed algorithm was tested in software simulation of EIT data and compared against a naive reconstruction technique. The entire cardiac EIT toolset was tested in a limited human trial. The experimental results show that the novel temporal ensemble averaging algorithm is able to isolate cardiac activity with accuracy consistent of the naive ensemble averaging technique but with greater temporal resolution.

To my husband who supported me throughout this endeavour.

Acknowledgements

I would like to thank Dr. Andy Adler, my thesis supervisor, for his support, guidance and patience throughout this thesis process. He was always available for input and guidance when I had questions or problems arose. He was incredible understanding in many situations when other people would have shown frustration. I am truly grateful.

I would like to thank Dr. Benjamim Chow and his team for access to their facility, patients, and time. Even though the cardiac imaging team always had a full schedule they each took the time to explain their process, help in volunteer recruitment, answer my questions, and prepare the data for use off site.

I would like to thank the volunteers who participated in this thesis research. They showed a great deal of kindness and patience. This was especially true when the Electrical Impedance Tomography (EIT) process was at its initial stages and things still needed to be ironed out. The volunteers at the University of Ottawa Heart Institute were at the end of a long fasting period and battled their hunger to volunteer for this study.

I would like to thank the Systems and Computer Engineering administrative team, technical support team and Nagui Mikhail for their generous support. The wonderful people in the office were there for any and all administrative issues. The technical support team were very accommodating in technical matters and procurement of supplies used in this research. Nagui Mikhail aided in the timely acquisition of hardware for this thesis research even though he was swamped with other requests.

Finally, I would like to thank my husband and friends who were there for support whenever it was needed. Whether there was a need for inspiration, a proof reader, a sounding board for ideas, a person to voice frustrations to, or a volunteer they were always there to aid.

Contents

List of Tables

List of Figures

List of Acronyms

ACE   Angiotensin Converting Enzyme

CAD   Coronary Artery Disease

CMRR   Common Mode Rejection Ratio

CT   Computed Tomography

DSA   Digital Subtraction Angiography

DSCT   Dual Source Computed Tomography

DSP   Digital Signal Processing

ECG   Electrocardiograph

EIDORS Electrical Impedance Tomography and Diffuse Optical Tomography Reconstruction Software

EIT   Electrical Impedance Tomography

FEM   Finite Element Method

HU   Hounsfield units

LDL   Low-Density Lipoprotein

LVER   Left Ventricle Ejection Ratio

NOSER Newton's One-Step Error Reconstructor

RC   Resistor-Capacitor

SNR   Signal To Noise Ratio

UOHI   University of Ottawa Heart Institute

USB   Universal Serial Bus

Chapter 1

Introduction

1.1 Motivation

Heart disease places a large burden on the Canadian health care system with a cost of $22.2 billion dollars every year [24]. In 2005, 3 percent of all deaths in Canada were caused by cardiovascular disease and currently, 5.7 percent of all Canadians have heart disease [24] [13]. The most common heart condition is Coronary Artery Disease (CAD) [13]. The main methods of diagnosis are: coronary angiography and Cardiac Computed Tomography (CT) [13]. Coronary angiography is a test where contrast agent is administered through the jugular artery while a sequence of x-ray images are acquired [8] [30]. Cardiac CT is a test where CT images are acquired of the cardiac region while a contrast agent is administered through a intravenous pump [13]. Coronary angiography is slightly more invasive (catheter placed in jugular artery for contrast agent) and involves radiation (X-ray imaging) [30]. Cardiac CT is less invasive (uses intravenous pump), uses a smaller dose of radiation for its x-ray imaging, and can produce 3D reconstruction of the heart [8] [13]. However, it is expensive, not all patients meet requirements (irregular heart beat, extensive arterial calcification, etc.) and the patient is subjected to radiation [8] [13]. For both

Angiography and CT the patient has to be scheduled for an appointment or time slot to receive imaging and the patient needs to be moved to the imaging facilities. EIT however would enable bedside monitoring of patients.

Electrical Impedance Tomography (EIT) is a low cost, non-invasive, and non-ionising medical imaging modality that has the potential to become a bedside available cardiac monitoring tool [29]. In order to achieve this goal, cardiac EIT must yield consistent and accurate results. EIT systems have improved through the past couple of decades and now possess better signal to noise ratios and very high frame rates [29]. Even though EIT still has inherent limitations such as low image resolution and poorly understood image artifacts, the improvements in technology, increased breadth of knowledge in the field, promising study results, and the need for safe monitoring solutions in the cardiac field has revived the pursuit of EIT studies in cardiac parameters [29].

1.2   Thesis Objectives

The purpose of this thesis is to create an EIT protocol that can be used at the University of Ottawa Heart Institute (UOHI) to investigate the potential of EIT imaging as it relates to cardiac function. To accomplish this goal the current CT protocol was studied, pre-existing EIT cardiac methodology was incorporated (breath hold, ECG gating, etc.), and a novel mathematical algorithm was utilised to take advantage of EIT temporal resolution.

The thesis has the following objectives:

- Produce an EIT and CT protocol to enable the retrieval of heart information such as heart blood flow and Left Ventricle Ejection Ratio (LVER) from EIT data

- Devise software and hardware setup to collect the data at the hospital and

analyse the data offline

- Design mathematical algorithm to facilitate imaging of perfusion in the heart with improved temporal resolution for more accurate imaging analysis

- Test imaging algorithm with a simulation in order to determine its usability and limitations

- Test imaging algorithm with patient derived data to analyse image temporal improvements (i.e. Can the heart be imaged?)

1.3   Thesis Outline

Chapter 2 of this thesis reviews background information on heart disease, diagnosis, and EIT. Chapter 3 describes the current cardiac CT protocol and proposes an EIT image collection protocol that can be performed in conjunction with current cardiac CT protocol. Chapter 4 describes the hardware and software design implemented to facilitate collection of EIT cardiac information and analysis offline. Chapter 5 presents the derivation of EIT temporal solver used in ensemble averaging and reconstructing the cardiac EIT images. Chapter 6 covers testing of the mathematical algorithm proposed in Chapter 5 using a known scenario and with collected patient EIT data. Chapter 7 summarises the technical contribution made in creation of the cardiac EIT protocol and suggestions are made for future work and use of the protocol.

Chapter 2

Background

2.1 Heart Disease

Heart disease is a group of conditions that limit the structure and function of the heart [25]. The human heart has the paramount task of pumping oxygenated blood through the body to feed all the living cells in the body [25]. There are many conditions that make up heart disease and they can be caused by either structural issues or blockages [25]. The most common of these conditions is coronary artery disease also known as coronary heart disease [31] [13]. Coronary artery disease is caused when fat, cholesterol, and calcium in blood forms a layer of plaque in the arteries (see Figure 2.1) [31]. This causes the arteries to narrow, reducing blood flow and increasing the chance of artery blockage [31] [25]. An artery can be blocked if the plaque thickens or blood clots form in the blood that can block the narrowed arterial pathway [31]. Coronary arteries act as a pathway that carry oxygenated blood travelling to the heart [31]. If this pathway is blocked the oxygenated blood never reaches the heart, which can cause a heart attack [31]. A heart attack occurs when parts of the heart muscle dies [31]. These arterial blockages can also cause heart failure and arrhythmia's [31]. Heart failure occurs when the heart muscle weakens and the heart no
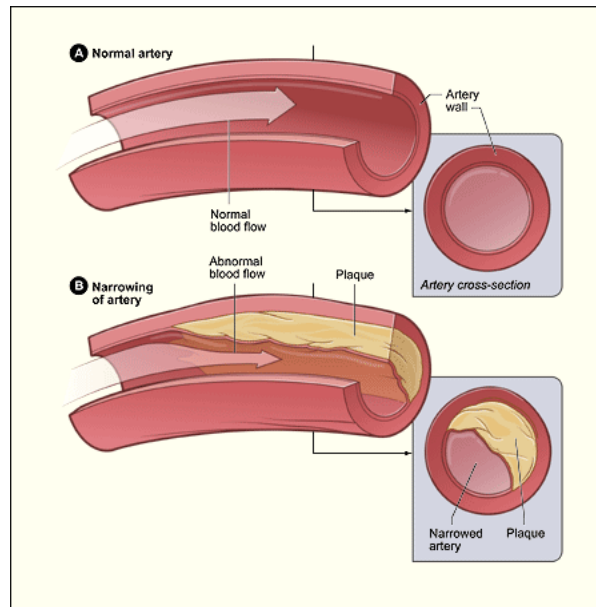
Figure 2.1: Healthy and Plaque Arteries (reproduced from [31])

longer has the ability to adequately pump blood through the body [31]. Arrhythmia is when the heart loses its natural rhythm, causing it to beat irregularly [31].

Early diagnosis of coronary artery disease can prevent a patient from developing a blockage of the artery [20]. This could potentially save their life. There are several treatments that can be administered once coronary artery disease is diagnosed. If the damage to the coronary artery is moderate a physician could prescribe medication to correct the damage and prevent further damage. Satins, niacin, fibrates and bile acid sequestrants lower Low-Density Lipoprotein (LDL) cholesterol and decrease deposits on the coronary artery. Aspirin is an anti-coagulant that reduces blood clotting and prevents artery blockages. Beta blockers ease the heart in pumping blood and decrease heart rate, blood pressure, and the heart's demand for oxygen. Nitroglycerin opens up the narrowed blood vessels and calcium channel blockers open coronary arterioles to increase blood flow to heart muscle. Finally, Angiotensin Converting Enzyme (ACE) inhibitors can also be administered and they are similar to beta blockers. Along or in lieu of medication a physician can suggest dietary changes which reduce further plaque build up as a preventative and maintenance measure. If the damage to the

coronary arteries needs immediate action and is too severe to be dealt with medication alone a physician can perform a surgical procedures to reduce blockage or re-route the blood.

2.2 Methods of Diagnosis

The gold standard in diagnosing coronary artery disease (CAD) is coronary angiography [13]. Angiography is an imaging technique used to visualise the flow of blood through the arteries, veins and heart chambers [8]. This is achieved by injecting a contrast agent through a catheter during an x-ray imaging sequence. The first step in coronary angiography is to administer local anaesthesia to the access site. Access to the blood vessels is made through the femoral artery (imaging the left part of the heart used in coronary angiography) or the femoral or jugular vein (to image the right side of the heart). Afterwards, a guide wire is inserted to keep the vessel open and the guide wire is threaded in into the desired location. A sheath is introduced to provide access for catheterisation. Finally a catheter is placed over the guide wire, and a small amount of radio opaque contrast agent is used to ensure that the catheter has reached the desired location. At this point the patient is ready to be imaged. During the imaging process additional contrast is administered and x-ray still images or motion images are taken. Digital X-ray still images are taken in several planes (seen in Figure 2.2) or a technique called Digital Subtraction Angiography (DSA) is used for motion images of blood flow [23].

DSA is a method used to subtract bones from X-ray images to allow for the path of a bolus of contrast agent through the vessel(s) of interest to be seen [23]. The DSA system is triggered by a computer timing signal which controls delivery of x-rays from the x-ray generator. X-rays are transmitted through the patient and are received by a signal intensifier. The x-ray image is then digitised. Once the image
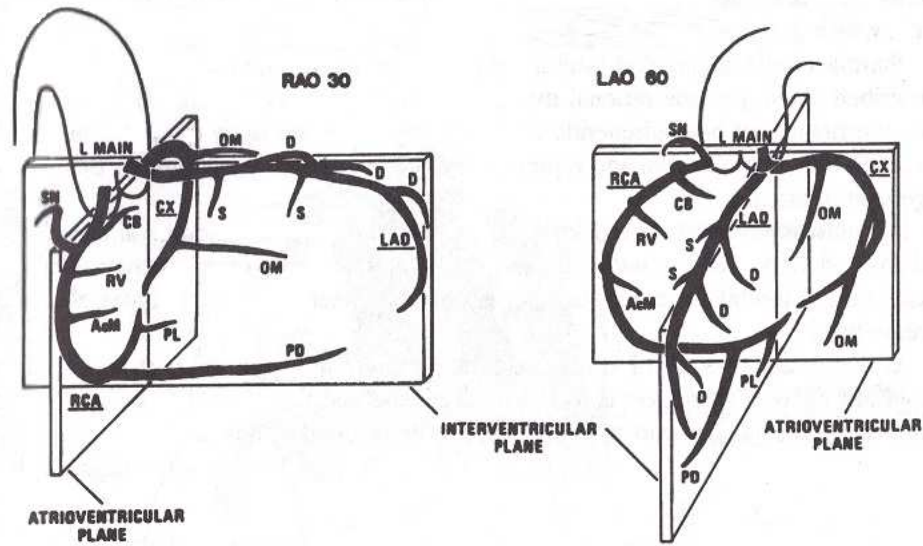
Figure 2.2: Anatomy of the heart as seen in each of the coronary angiographic planes (reproduced from [8])

train is in memory it can be processed in several ways. The simplest and most often used method is called temporal subtraction. In temporal subtraction the image set taken without contrast is subtracted from the set taken with contrast. This method is prone to movement artifacts and cannot be directly used for cardiac imaging. Image registration techniques have been researched for cardiac imaging [32]. Image registration is performed in two steps. First a method is used to find the correlation between two images (pixels, control points, etc) and then the necessary corrections are performed to align one image to another. After registration of images the temporal subtraction method can be used. Both still and DSA x-ray imaging techniques allow the medical practitioners to identify blockages due to lack of blood flow as gaps in contrast agent in the x-ray images indicate blockage (see Figure 2.3 part b) [8].

There are many risks associated with angiography. These include: bleeding, infection, pain at catheter insertion sites, allergic reaction to contrast agent, arrhythmia, damage to kidneys from contrast agent, blood clot formation at the insertion site (could cause blockage of artery and heart attack), fluid build up around the heart which could prevent proper function, and exposure of the patient to a dose of radia-
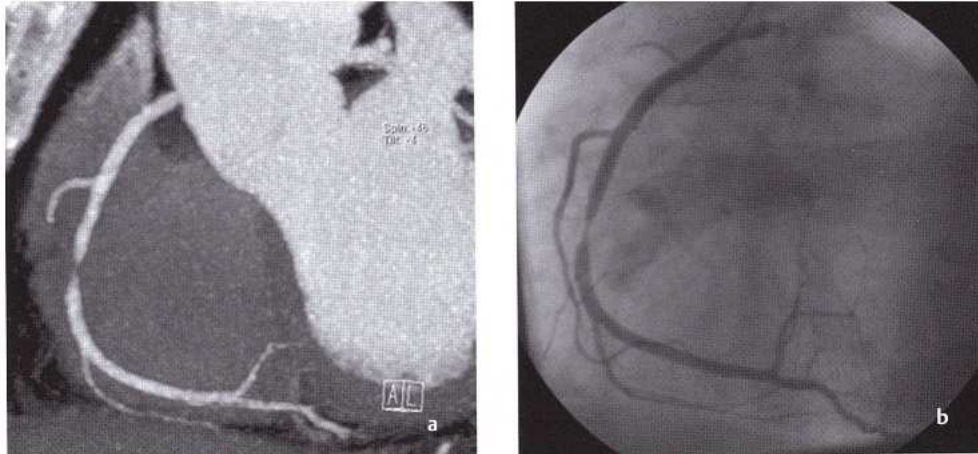
Figure 2.3: a)CT image versus b)Angiography image depicting stenosis (blockage) in artery (reproduced from [8])

tion [30] [8].

The University of Ottawa Heart Institute and several other institutions have moved towards the use and research of less invasive techniques such as cardiac computed tomography [13]. Cardiac computed tomography produce 2D and 3D x-ray images taken around a single axis [8] [10]. Computed tomography systems work on the principle that an X-ray beam that passes through the body gets attenuated along its path. Each x-ray is detected and an algorithm of backprojection is used to calculate the voxels attenuation co-efficient. Relative attenuation is measured in Hounsfield units (HU) where $-1000HU$ represents air, and $0HU$ represents water. Compact bone is around $1500HU$. A windowing technique is used to associate the HU units to 256 colours of the grey scale.

Computed tomography has been a gold standard for imaging other areas of the body such as extra cranial, thoracic, abdominal vascular distribution, aorta, pulmonary arteries, great vessels, renal and peripheral arteries; but until the 1990's its slow image acquisition rate has prevented its use in imaging the heart [8] [10]. The invention of helical CT and multidetector CT's in the nineties brought higher image acquisition rates that could handle the speed of motion of the heart.
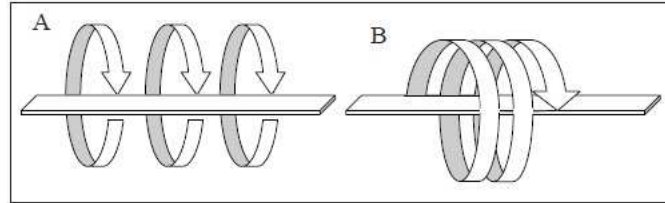
Figure 2.4: CT Scan Path of Classic CT scanners versus Helical CT scanners (reproduced from [13])
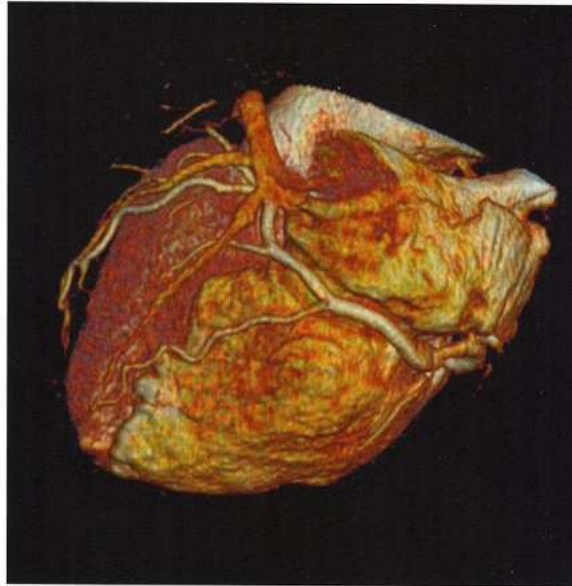
Figure 2.5: Volume rendered image from 64 slice CT (reproduced from [8])

With the invention of slip ring technology came the helical CT, which, combines continuous detector rotation with continuous table movement [8] [13]. The data is collected in a spiral path allowing for the imaging of volumes. Figure 2.4 depicts the path of a helical CT scanner and Figure 2.5 shows an example of volume reconstruction capability. This form of CT cut down on acquisition time significantly, since the table does not have to be stationary for CT image acquisition and acquisition is continuous. For example, CT image acquisition of the thorax used to take several breath holds but now it can be scanned in one breath hold. Figure 2.6 is an image of a current helical CT scanner.

The Multidetector CT was invented in 1999 [8] [13] [10]. The first one had 4 detector rows, with a gantry rotation of $500ms$ per rotation, which made Electrocardiograph
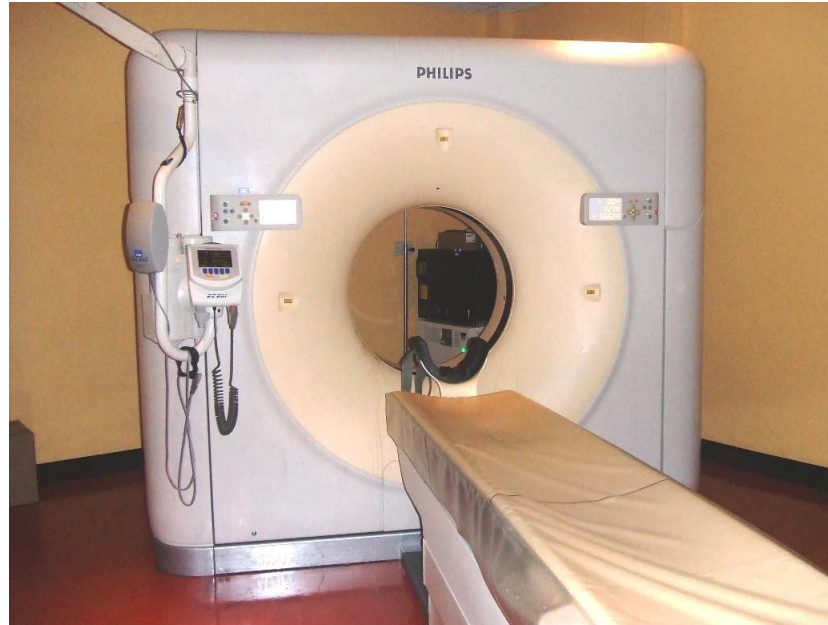
Figure 2.6: 64 Slice CT Scanner (reproduced from [39])

(ECG) triggered imaging of the heart possible. Scan times were cut down from 10 or 15 minutes to 30 to 40 seconds and image slices were reduced to between $1mm$ and $1.25mm$ thickness. CTs with 16 detector rows were soon to follow with a gantry rotation of $420ms$ per rotation, acquisition time of 20 seconds and slices that were $0.75mm$ to $0.5mm$ of thickness. In 2004 CT scanners with 64 detector rows were introduced (shown in Figure 2.7) with gantry times of $330ms$, a short acquisition time of $10s$, and image slices of $0.5mm$ thickness. Thinner image slices meant sub-millimeter spacial resolution, which is desired for cardiac CT, and overlapping slices for better image reconstructions. The reduction in acquisition time means less opportunity for patient movement during breath hold, reducing the chance of movement artifacts. The temporal resolution of a CT scanner is calculated to be around one half of the gantry rotation time. Therefore, the temporal resolution of a 64 slice scanner is around $165ms$. This temporal resolution is adequate to produce motion free image during diastole; but to produce motion free images during systole a temporal resolution between $50ms$ to $100ms$ is desired. There are several reconstruction algo-
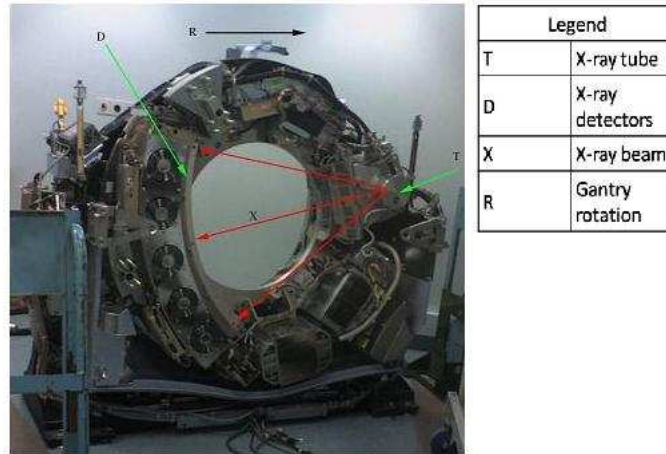
Figure 2.7: Internals of a 64 Slice Scanner (reproduced from [40])

rithms that are designed to improve the temporal resolution of the CT images, one of which is segmented reconstruction. Since images are taken for several cardiac cycles this method is very sensitive to fluctuating heart rates. In 2007, 256 detector ring scanners started their testing phase. Hopefully when they become available they will improve the temporal resolution of cardiac CT. Also, in 2006 Dual Source Computed Tomography (DSCT) scanners were invented. DSCT are designed with two tubes and detectors 90 degrees from each other. Some studies show that DSCT can produce a temporal resolution of about $83ms$.

There are two forms of ECG gating used in Cardiac CT [13]. Prospective electro-cardiographic gating is when the image acquisition is ECG triggered at a predefined time after R wave (shown in Figure 2.8 part A). This form of ECG gating allows the patient a smaller dose of radiation but comes as a cost to image resolution since it is quite sensitive to motion artifact. This motion artifact can be seen in Figure 2.9 part B. In order to reduce motion artifacts some patients have to be given medications such as beta blockers or calcium channel blockers in order to bring their heart rate in an acceptable imaging range of below 65 beats per minute. Another form of ECG gating is known as retrospective electrocardiogram gating is performed by averaging the reconstructed CT images over several heart cycles (shown Figure 2.8 part B).
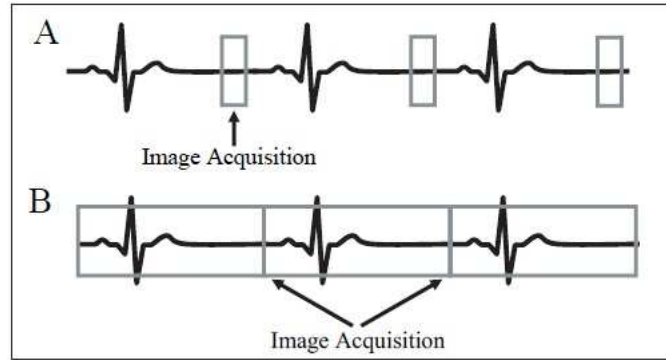
Figure 2.8: ECG Gating Protocols: A. Prospective electrocardiographic gating B. Retrospective electrocardiographic gating (reproduced from [13])

This method allows for an improvement in acquisition speed and spacial resolution in the through plane but the patient receives more radiation.

A contrast agent is required in cardiac CT since soft tissue, muscle, myocardium, blood, thrombus and fibrous tissue are all close in HU units and receive identical or similar grey scale value, making it difficult to distinguish between them without a contrast agent [8]. It is important in cardiac CT to distinguish between the wall and blood pool of the ventricles and other chambers of the heart.

Cardiac CT has several limitations. Patient motion during breath hold could cause motion artifacts (respiratory artifact), heavy vascular calcification as shown in Figure 2.9 part A, beam hardening caused by contrast material building up in the superior vena cava (Figure 2.9 part A), stair step artifact caused by arrhythmias (2.9 part B), coronary stents and pacemaker electrodes all cause image artifacts [13] [8]. CT scanners are relatively expensive and cannot be used for monitoring purposes.

There are risks to undergoing CT coronary angiography as well. The procedure administers a radiation dose of $5mSv$ to $12mSv$ [13]. This is high considering a chest X-ray is about $0.06mSv$ and background radiation per year is around $3.6mSv$ [15]. The patient might experience adverse reaction to medication such as the beta blockers and contrast agent that might be administered. CT scanners are loud. Because the detector is limited in size, people with claustrophobia might feel discomfort. The
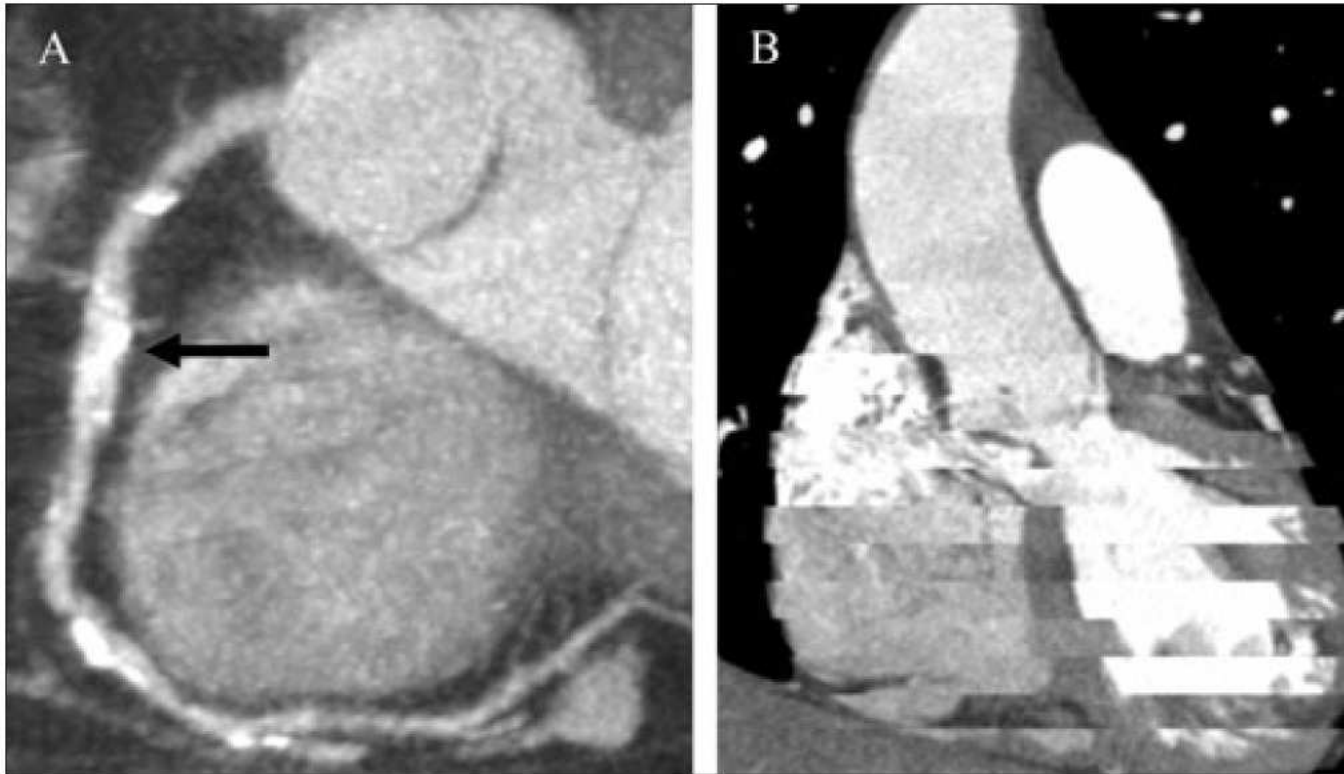
Figure 2.9: CT Artifacts: A. Calcification and beam-hardening artifact. The arrow indicates significant coronary calcification obscuring the lumen of the coronary artery. B. Effect of arrhythmia in ECG gated image reconstruction. The frequent premature ventricular contractions cause stair-step artifact (reproduced from [13]).
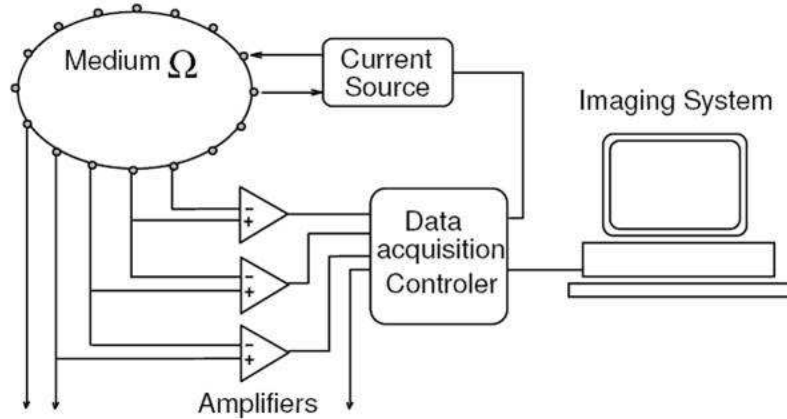
Figure 2.10: EIT Block Diagram (reproduced from [2])

intravenous site has to be monitored to verify that blood clotted properly around area.

2.3   Electrical Impedance Tomography

Electrical Impedance Tomography (EIT) is an experimental medical imaging technique which was founded in 1978 [26]. Before its use in medical imaging, EIT was used in geophysics applications [9]. This form of imaging uses a set of electrodes placed on the body as source and receiver in which a pattern of alternating current is applied [26]. The conductivity distribution is measured by the receiving electrodes and using mathematical calculation an image is inferred. A block diagram of a typical EIT system can be found in Figure 2.10. EIT works on the principle that conductivity varies between tissue types and when organ and tissue in our body undergo normal physical changes. For example, lungs are less conductive when filled with air.

There are two main schools of thought when it comes to electrode placement in EIT [33]: Pair Drive and Trigonometric Current Patterns. In Pair Drive tomography a ring of 16 electrodes and a single current generator is used as shown in Figure 2.11. In this method a current is passed between two adjacent electrodes and the resulting voltage distribution is measured by all remaining electrodes. This method is used in
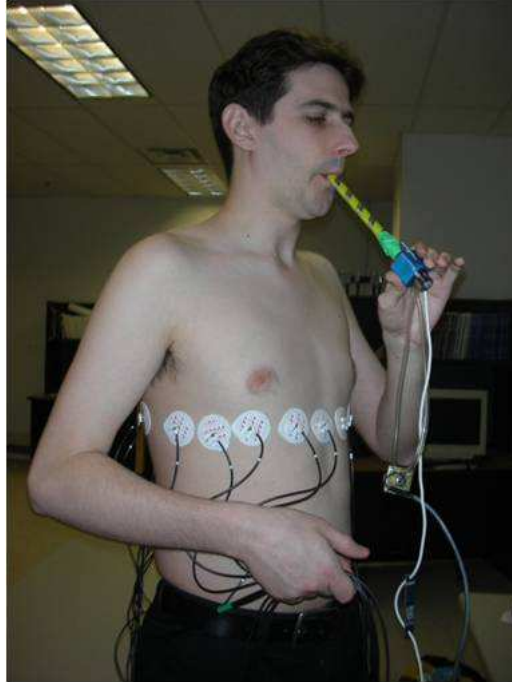
Figure 2.11: 16 Ring EIT Electrode Setup

this thesis. The advantage of this method is its robust design, but the drawbacks are that it is sensitive to electrode error and only changes in voltage distribution can be imaged. With Trigonometric Current Patterns tomography there are 32 or 64 electrodes used and each electrode has its own current generator. The increase in the number of electrodes gives this method a better spacial resolution and it is slightly less sensitive to electrode errors. But it also makes this method more complex.

EIT imaging is more difficult to reconstruct than modalities such as CT [19]. CT, as mentioned in the previous section, uses a collimated x-ray beam which directs x-rays in a straight path through the target. Therefore, each measurement in CT depends on a limited set of voxels in its path. In contrast an applied current at one location effects measurements at all electrodes on the body. Therefore, each voxel depends on all the other voxels and many simultaneous calculations have to be made to reconstruct the EIT image. This makes the EIT reconstruction problem ill conditioned and EIT measurements are more sensitive to the area under the electrodes

versus the centre of the image. In 1902 Hadamard defined ill posed as a problem
that does not meet the following three criteria: has one solution, solution is unique,
and solution depends on data. There are many different reconstruction techniques for
EIT and researchers are constantly working to better the models and solutions. The
main reconstruction techniques include a historical backprojection algorithm where
voltages are projected along equi potential lines and regularised imaging solutions.
Regularised imaging uses a linear forward problem. A Jacobian sensitivity matrix
based on conductivity and movement can also be used. This technique utilises an
inverse solution that incorporates a noise model, conductivity prior and movement
prior [5]. For this thesis an open source software called Electrical Impedance Tomog-
raphy and Diffuse Optical Tomography Reconstruction Software (EIDORS) is used
which incorporates all mentioned reconstruction techniques. The regularised recon-
struction method is used to obtain the EIT images prior to temporal reconstruction
methods derived for this thesis.

Regularisation utilises a priori information and a penalty function to allow for a
solution to the EIT ill conditioned problem. Chapter 5 section 5.4.1 explains and
derives regularisation in detail. Regularisation equations are briefly introduced in
this section. For small changes in conductivity the relationship between $\mathbf{x}$ and $\mathbf{y}$ is
linear [7]. Therefore, the linear forward problem used for EIT image reconstruction
is shown in equation 2.1. $\tilde{\mathbf{n}}$ represents measurement noise and $\tilde{\mathbf{J}}$ represents a Jaco-
bian matrix calculated from a finite element method. There are several regularisation
techniques that can be implemented to derive an EIT inverse equation. Tikohonov
regularisation was chosen for this thesis. Using Tikohonov regularisation the inverse
solution (equation 2.4) is derived from minimising the sum of quadratic norms (equa-
tion 2.3). Where $\bar{\mathbf{x}}$ represents expected value of conductivity changes, which becomes
zero in difference EIT. $\Sigma_{\tilde{\mathbf{n}}}$ is the covariance matrix of measured noise. In equation 2.4
λ refers to the regularisation parameter which represents the trade off between reso-

lution and noise. EIT measured data is more sensitive to boundary elements, in an attempt to compensate, matrix $\mathbf{R}$ is scaled with the sensitivity of each element.

$$
\begin{bmatrix} \mathbf{y}_1 \\ \mathbf{y}_2 \\ \vdots \\ \mathbf{y}_N \end{bmatrix} = \begin{bmatrix} 0 & \mathbf{J}_1 & \cdots & 0 \\ \vdots & \vdots & \cdots & \vdots \\ \vdots & \vdots & \cdots & \vdots \\ 0 & 0 & \cdots & \mathbf{J}_N \end{bmatrix} \begin{bmatrix} \mathbf{x}_0 \\ \mathbf{x}_1 \\ \vdots \\ \mathbf{x}_N \end{bmatrix} + \begin{bmatrix} \mathbf{n}_0 \\ \mathbf{n}_1 \\ \vdots \\ \mathbf{n}_N \end{bmatrix} \tag{2.1}
$$

and also as

$$
\tilde{\mathbf{y}} = \tilde{\mathbf{J}}\tilde{\mathbf{x}} + \tilde{\mathbf{n}} \tag{2.2}
$$

$$
\varepsilon^2 = ||\tilde{\mathbf{y}} - \tilde{\mathbf{J}}\tilde{\mathbf{x}}||^2_{\Sigma_{\tilde{\mathbf{n}}}^{-1}} + ||\tilde{\mathbf{x}} - \bar{\mathbf{x}}||^2_{\Sigma_{\tilde{\mathbf{x}}}^{-1}} \tag{2.3}
$$

$$
\mathbf{B} = \left(\tilde{\mathbf{J}}^t \mathbf{W} \tilde{\mathbf{J}} + \lambda^2 \mathbf{R} \right)^{-1} \tilde{\mathbf{J}}^t \mathbf{W} \tag{2.4}
$$

There are drawbacks to regularisation such as a trade off between resolution and noise. Therefore, resolution on EIT images is low (2-3 cm in cross sectional plane) [29] and boundaries in images contain errors [7]. Also, the spatial resolution of EIT is limited by the number of electrodes used. The greater the number of electrodes imaging an area the more measurements are obtained for the area. Allowing for an increase spatial resolution of the area in the EIT image. The EIT system used for this thesis has a limit of 16 electrodes for measurements therefore limiting the spacial resolution. EIT images, as seen in Figure 2.12, more closely resemble nuclear imaging modalities rather than high resolution images from CT. This technology is not meant as a means to pinpoint the exact location of an internal problem. Rather its goal is to be used as a bedside monitoring tool to identify if a problem exists. EIT is being studied for several biomedical imaging applications such as lung perfusion, thorax, GI tract, breast cancer, and heart [5]. In regards to cardiac research the biological
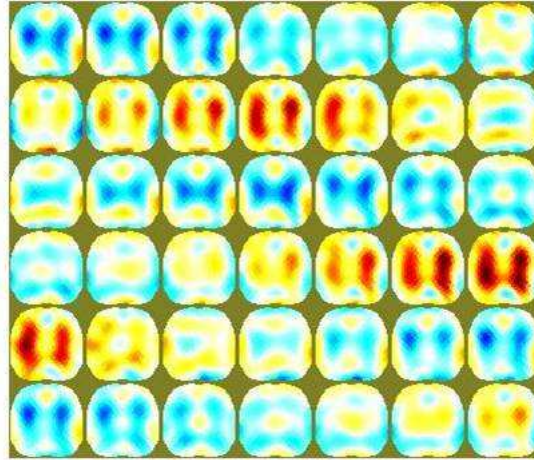
Figure 2.12: Example EIT Images taken with GOE MF II system of patient supine while breathing at a normal rate. The images were reconstructed using EIDORS software and a subset of two breathing cycles is shown (exhalation, inhalation, exhalation, inhalation, exhalation). The colour red represents regions of high conductivity while blue represents regions of low conductivity. The earliest time interval is top left, time progresses left to right and top to bottom. The time interval between each image is approximately .024 seconds

parameter of stroke volume has shown to be a useful diagnostic marker for heart failure, hypertension and cardiovascular diseases and recent research has shown that EIT has great promise in predicting this parameter [29].

EIT has limitations. It has a high sensitivity to measurement noise (electrical and geometrical), high sensitivity to electrode placement (number of electrodes, electrode size, distance between electrodes) and movement, low spacial resolution (2-3 cm in cross sectional plane), and image reconstruction is complex (ill posed, non linear). Difference EIT only images relative changes in the underlying tissue [29]. These inherent limitations cause the following issues or difficulties that need to be overcome regarding cardiac EIT imaging: Low Signal To Noise Ratio (SNR), frequency overlap, spatial overlap, and calibration drift [29]. Low signal to noise ratio refers to the fact that cardiac related signal is a low amplitude component of the EIT signal compared to changes in larger organs such as the lungs and the noise level of the EIT signal.

This occurs because the heart is compressed by the lung pressure during each breath cycle. This heart compression modulates the heart function and changes its volume and pressure, adding a lung frequency contribution to the cardiac signal. The ECG gating algorithm cannot fully eliminate this lung contribution. EIT has low spacial resolution, causing spatial overlap in heart anatomy on EIT images. This makes distinguishing cardiac activity in specific anatomical regions a great difficulty. Finally, calibration drift describes how stroke calibration is dependent upon the health of the lung and cardiac muscle. If a patient presents with certain conditions, such as lung edema, stroke volume becomes difficult to calibrate.

EIT also has many advantages; it is non-invasive, portable, non-ionising, and has good temporal resolution [5]. These advantages outweigh the disadvantages in many applications and propagates the advancement and research in EIT technology. These advances in technology and research have addressed many of the cardiac related EIT limitations [29]. For instance EIT hardware now boasts improved signal to noise ratios and higher acquisition rates (up to 1000 frames/second) [16]. Several EIT measurement protocols have been devised to allow for EIT stroke volume determination such as breath hold, ECG gating, temporal spacial domain, and the use of contrast agents [29]. The first of the methods is the breath hold which is used to reduce the ventilation component of the EIT signal. Unfortunately a subject can only hold their breath for a relatively short period of time and this method cannot be used for long term monitoring. The ECG gating method allows the subject to breath during signal acquisition by averaging EIT data over several heart cycles to extract the cardiac related impedance signal. If this method is used while the subject is breathing, a minimum of 100 averaged cardiac cycles are required to sufficiently remove the ventilation component from the cardiac component. There are two main disadvantages to this method. If the patient ventilation signal is a multiple of their heart rate the ventilation signal cannot be completely removed from the cardiac signal. The other

is that this method introduces a temporal delay. Frequency domain separation in the temporal and spatial domain is the third method and draws on the theory that the cardiac and respiratory signals are separated in the frequency domain. Using filtering frequencies can be separated and the ventilation component removed. The minor disadvantage to this method is that there is still an addition of a small delay. Finally the use of contrast agent such as hypertonic saline increases the amplitude of the cardiac signal and therefore allows for better cardiac and ventilation distinction. Yet the administration of the contrast agent introduces an invasive component to the non invasive EIT imaging protocol.

Several mathematical algorithms have been derived to obtain stroke volume from the EIT measurements [29]. Two accepted methods of cardiac output measurements are thermodilution (dye is injected intravenously and amount of dye diluted in blood is measured at another down stream) and impedance cardiography (4 electrodes are used to measure changes in the thorax). These methods were used as control comparisons for two novel EIT mathematical approaches for calculating cardiac output. These new approaches managed to achieve a high correlation equal to 0.86 compared to the control. This correlation is quite high compared to previous studies. The two methods are impedance time curves and parametric EIT. Impedance time curves method uses 200 averaged heart cycles to determine the width and height of impedance time curves and using those parameters stroke volume can be calculated. The parametric EIT method uses an impedance model of the thorax in which a $2D$ ellipsoids represent the heart region. This $2D$ ellipsoid is optimised for each individual using their MRI scan to fit their heart region and then stroke volumes are calculated from changes in this region.

2.4 Summary

The intention of this thesis is to develop hardware and software tools for a cardiac

EIT research study at the University of Ottawa Heart Institute. Several of the accepted research methods from previous cardiac EIT studies have been implemented in this thesis such as the breath hold and ECG gating to filter out the ventilation component of the EIT signal. This thesis also develops a novel temporal ensemble averaging method to take advantage of EIT's high temporal resolution. Since by the end of this thesis the study is still at its infancy; the images obtained by these methods will be quantitatively studied in order to acquire interest into further development of this study. No attempt to calculate stroke volume from images is made in this thesis and this is left for future work. Many of the previous cardiac EIT studies have been performed on healthy subjects, therefore the continuation of this research can shed some light and answer or direct one to new challenges in cardiac EIT as it pertains to patients that have the greatest benefit from this biomedical technology.

Chapter 3

Hardware

One of the goals of this thesis is to develop a protocol in which the images from the two different imaging modalities Computed Tomography (CT) and EIT. CT and EIT images are quite different in nature and appearance, increasing the difficulty of direct comparison between these image modalities. During the CT procedure in this thesis CT images are taken concurrently with ECG readings from the subject. If the EIT measurements are in turn taken concurrently with ECG readings then the common ECG readings would allow for QRS cycle image synchronisation between CT and EIT measurements. The human heart has minor variability between each heart beat. Therefore, the images acquired from CT will not be perfectly registered to the ones acquired by EIT. The heart will undergo similar changes within each heart beat and cardiac parameters such as cardiac output should yield similar results. Therefore, only specific PQRST cardiac regions can be studied between the two modalities.

In order to enable concurrent ECG and EIT measurements there was a need for the development of several auxiliary circuits and use of off the shelf devices. Figure 3.1 depicts the hardware setup that was chosen for this thesis. The hardware setup includes a GOE MF II EIT system to take the EIT measurements from the patient, an ECG amplifier to amplify the cardiac signal, and a PicoScope oscilloscope which
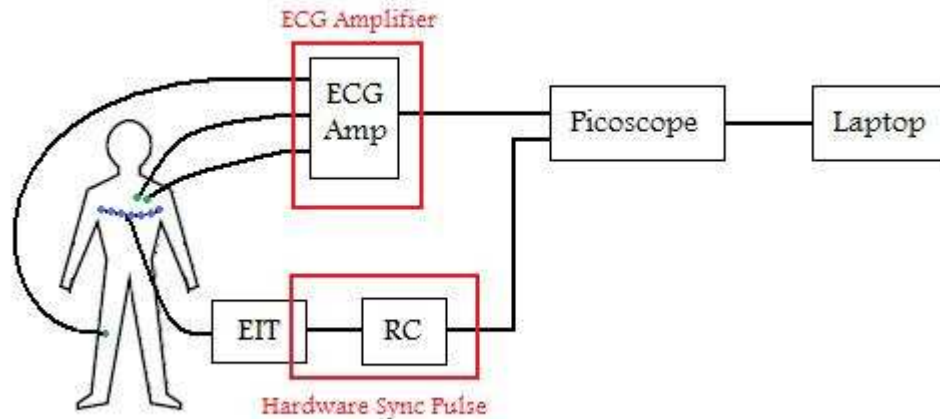
Figure 3.1: EIT Hardware Setup

allows for the visualisation of the signal. An Resistor-Capacitor (RC) circuit connect the EIT system to the oscilloscope and acts as a hardware sync pulse between the ECG data and the EIT data. The PicoScope is attached to the laptop which saves the signals from the oscilloscope. The components found in the red boxes (ECG amplifier and RC circuit) were designed and built for this thesis application while the rest of the components (EIT system, PicoScope, and laptop) were previously purchased.

3.1   ECG Amplifier Design

The heart is a powerful muscle that uses strong contractions to pump blood throughout the body [4]. These contractions produce electrical potentials that can be measured throughout the body and at its surface. The stage of muscle contraction can be determined from the resulting PQRST wave shown in figure 3.2. The P stage represents the depolarisation of the SA node and the spreading of the blood from the right atrium to the left atrium (atrial contraction). The QRS complex represent the atrial depolarisation and ventricular contraction. The T wave represents the
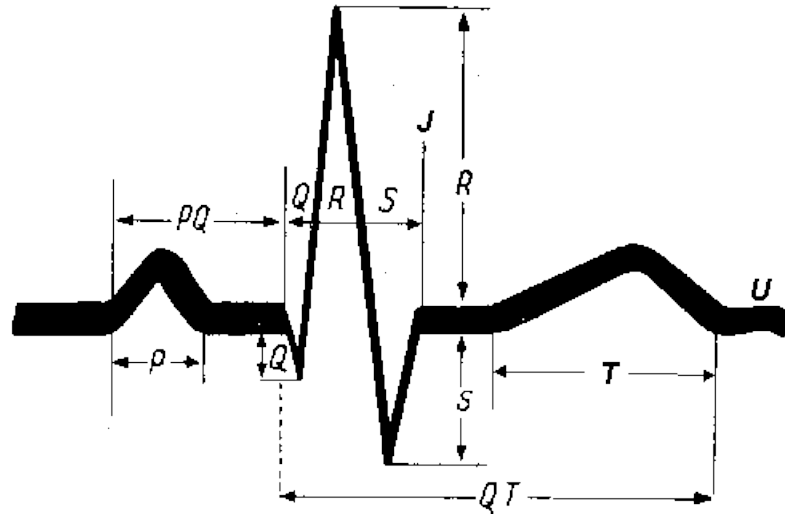
Figure 3.2: Sample PQRST Heart Signal (reproduced from [37])

re-polarisation and recovery of the ventricles.

There are several challenges inherent in measuring the PQRST signal. When two electrodes are placed far apart on the body, they will experience a constantly changing potential created by the epidermis [11]. Also, lead wires can act as an antenna receiving unwanted 60 Hz signal from the mains supply. Motion artifacts are also common. Therefore, the amplifier used in this circuit must have high input impedance in order to minimise loading of the signal being measured [14, 3, 11]. High gain (>1000) is also required in order to properly display and record the small surface heart signal [11].

Several safety issues have to be addressed as well when designing any electrical circuits that are directly connected to a patient [11, 14]. The power sources used for the circuitry can be a shock hazard to the patient. Ground loops can exist if more than one electrical device is grounded to the patient at the same time in different locations. The slight potential difference between the two grounds could generate a dangerous current though the patient.

This circuit was designed with the above mentioned measurement and safety chal-
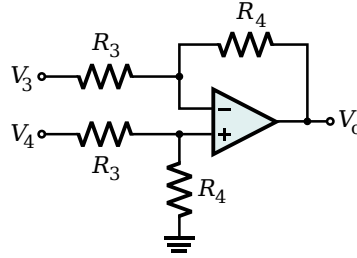
Figure 3.3: Single op amp differential amplifier circuit (reproduced from [14])

lenges in mind. In order to measure heart signal while rejecting noise that exists at both electrodes a desired amplifier must have a high input impedance and Common Mode Rejection Ratio (CMRR) [3, 14, 34]. Figure 3.3 illustrates a single operational amplifier (op amp) differential amplifier circuit. Using Ohm's Law and superposition the differential gain, common gain, CMRR, and input impedance of this circuit can be determined. The differential gain $A_d = R_4/R_3$. The input impedance R_{in} is given by $2R_3$. If a high differential gain (A_d) is desired then resistor R_3 has to be small. Decreasing R_3 decreases the input impedance of the circuit. From the circuit analysis it is evident that a single op amp design has two major drawbacks of a low input impedance and a difficult to alter differential gain.

Figure 3.4 illustrates a typical three op amp differential circuit often used in instrumentation amplifiers [14, 34]. The differential gain for this circuit A_d is equal to $(2R_2+R_1)/R_1$ and the common mode gain A_c is 1, allowing for simplified manipulation of differential gain by resistor R_1. Both op amps in stage one are non inverting resulting in a high input impedance (ideally infinite). This circuit also boasts a high CMRR. In order to attain this high CMRR all the gain has to be attained in stage one while stage two is designed to have a differential gain of 1. In this way, stage two is used as a differential amplifier for the input voltages (v_3 and v_4) from stage one rejecting their common mode difference and therefore producing a low CMRR. The instrumentation amplifier overcomes the drawbacks of the one op amp differential
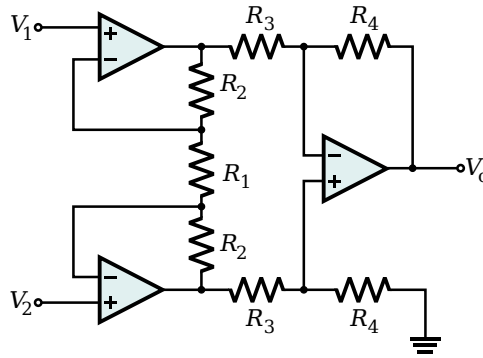
Figure 3.4: Three op amp differential amplifier circuit (reproduced from [14])
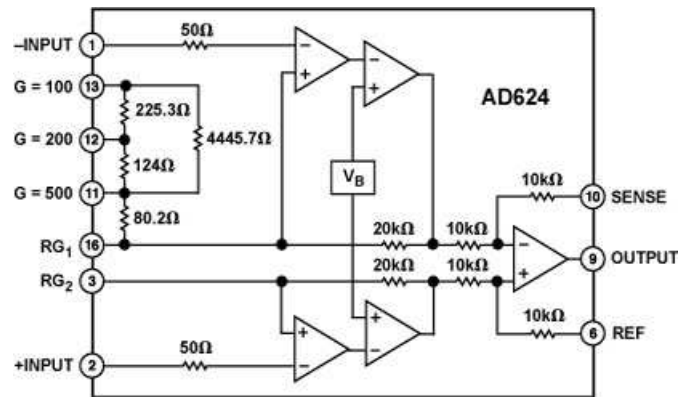
Figure 3.5: Instrumentation Amplifier AD624 Block Diagram (reproduced from [17])

circuit and exhibits all the design characteristics for the ECG amplifier.

An AD624AD instrumentation amplifier was selected for use in the ECG signal (see figure 3.5). The AD624 has the following specifications: High CMRR of up to 130 dB, Low Input Offset Voltage of 25 μV max, Low Input Offset Voltage Drift of 25μV$/$°C max, and a high gain of up to 1000 [17].

As stipulated, several safety issues have to be addressed as well in this design since the electrodes provide an excellent current path through the body. To limit the likelihood of the patient receiving a shock from the power source, 9V batteries were used as a power supply [11, 3, 37, 14]. As an additional measure two oppositely biased diodes were placed on the leads to shunt voltage swings greater than .6 volts to ground. The signal of interest is expected to be less than 5 millivolts and should not effect the diodes. Further circuit protection could have been provided through
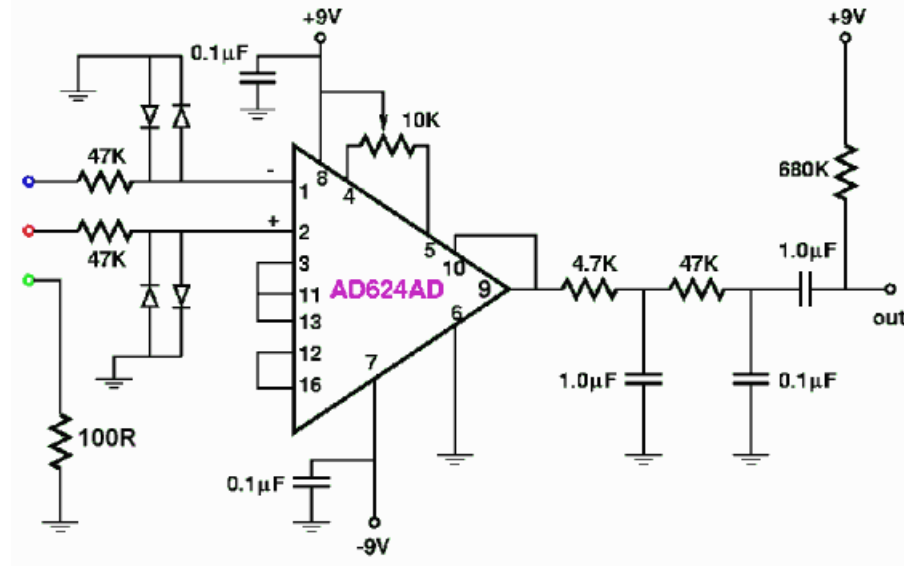
Figure 3.6: Electrical Cardiograph Amplifier Schematic (reproduced from [11])

the use of opto-isolators and other isolation circuitry. This option would have been utilised had we chosen to use a 120V power supply versus batteries.

The heart signal consists of positive and negative components. This circuit was originally designed for an Analog to Digital converter with a single supply input range [37]. Therefore a circuit divider was placed on the output to pull up the signal by 2V. The ECG Amplifier schematic implemented is shown in figure 3.6.

The ECG amplifier was tested to observe proper operation and its ability to reject EIT hardware interference. Figure 3.7 shows the ECG signal before EIT system is turned on the ECG signal and the different sections of the QRS complex are clearly visible. The ECG gating method used in this thesis uses R wave detection. Figure 3.8 shows the ECG signal after the EIT system is turned on and acquiring data. The EIT hardware interference is evident but fortunately for our purposes the R wave remains clearly detectable during EIT acquisition.

3.2 Picoscope Oscilloscope Specifications

A compact PicoScope 2204 Universal Serial Bus (USB) oscilloscope was chosen

ECG Amplifier Signal Without EIT Hardware Interference
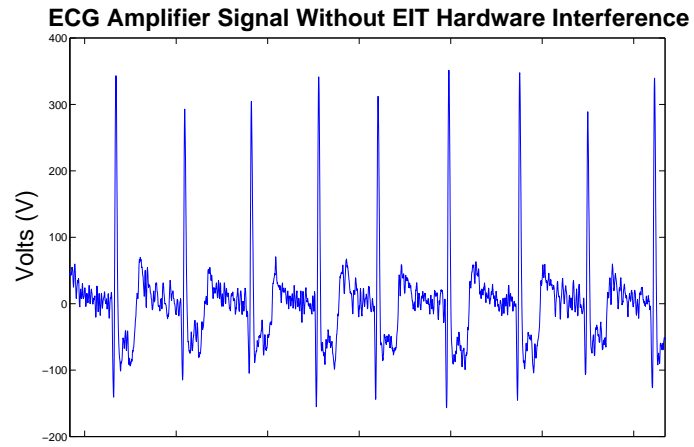
Figure 3.7: ECG Amplifier signal without EIT hardware interference.

ECG Amplifier Signal With Hardware Interference
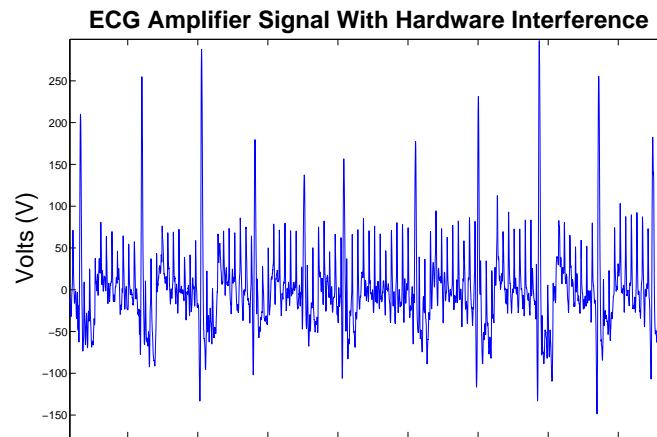
Figure 3.8: ECG Amplifier signal with EIT hardware interference.

to capture the ECG amplifier and RC sync pulse signals. The reasons for choosing a USB oscilloscope was the EIT system and all of the accompanying devices need to be portable and safe. This oscilloscope not only met the form factor requirement but it's operational specifications are desirable as well. The Picoscope 2204 boasts 2 input channels, a $10Hz$ bandwidth, a sample rate of $100MS/s$, and an $8kS$ memory buffer [38].

3.3 EIT System Specifications

The GOE MF II EIT system was chosen for this thesis. The EIT system is approved for human research. The EIT system uses pair drive tomography (16 electrodes one current source) as described in the background section 2. The current is passed between a pair of adjacent electrodes (starting from electrode 1 and 2) readings are obtained from the remaining electrodes before the current is passed between the next electrode pair (stimulation is performed in a counter clockwise direction). The system default frame rate of 13 frames per second is implemented to obtain the 256 measurements per frame. Each EIT measurement cycle is of 30 second duration.

3.4 EIT Hardware Sync Pulse Design

Hardware synchronisation of the ECG signal to the EIT data was desired to avoid delays that might be introduced in a software implementation. The GOE MF II EIT system did not already possess this functionality and a hardware sync pulse circuit needed to be implemented. The GOE MF II EIT system uses a SBC62 DSP-Board. Based on advice from the manufacturer, several pins were tested on the 40 pin connector of the Digital Signal Processing (DSP) board and it was found that Pin 14 produces a square pulse train for the entire duration of measurement. The information of interest is the initiation and cessation of the measurement. Each pulse was of very short duration and the frequency of the pulse train was higher than the acquisition
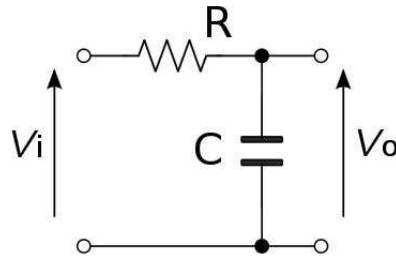
Figure 3.9: First Order RC Circuit($R = 2.2M\Omega$, $C = 1000pF$, and $\tau = 0.002s$)

rate of the oscilloscope. As such a simple RC circuit shown in figure 3.9 was designed as a low pass filter for the individual frame pulses throughout the measurement cycle. A low pass filter attenuates all high frequency components that are above its cut off frequency measured by the RC time constant. A resistor value of $R = 2.2M\Omega$ and a capacitor value of $C = 1000pF$ was used to yield an RC time constant of $\tau = 0.002s$. Without the low pass filter the oscilloscope would miss most of the pulses in the pulse train. The low pass filter attenuates these pulses and smoothes the signal allowing for start and end determination of the sync pulses. The input Vi is the input from pin 14 from the EIT system and the output Vo is fed into the PicoScope oscilloscope. Figure 3.10 shows the sync pulse signal as seen with the PicoScope. Instead of one smooth transition step up and one smooth transition step down there are several steps in the signal. The PicoScope saves each several thousand samples in separate excel files. The part of the signal in each file had a different auto magnitude scale. Therefore, when the files are patched together to obtain the full signal there are fluctuations in magnitude.

3.5   Summary

Since the GOE MF II EIT system lacked simultaneous ECG measurement an ECG amplifier and a method of synchronisation were designed to add the needed functionality. Figure 3.1 shows the overall hardware setup used in our EIT protocol.
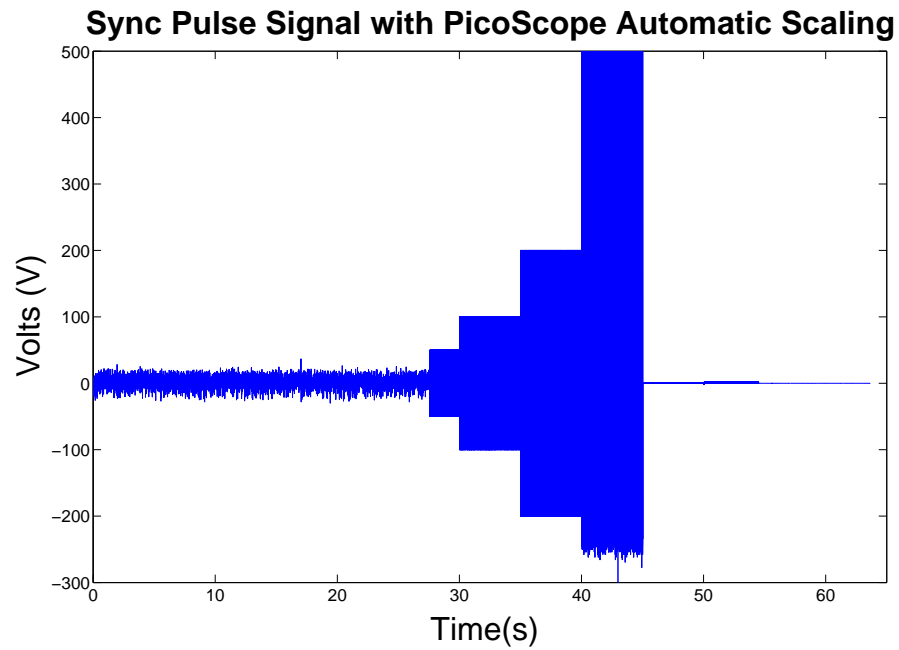
Figure 3.10: ECG Sync Pulse signal without EIT hardware interference. The sync pulse signal is not uniform amplitude due to the auto ranging behaviour of the Picoscope. The signal is pieced together from 10 or more separate files each with a different scaling range.

Chapter 4

Computed Tomography and EIT Procedure

To image inside of the blood vessels, arteries and chambers of the heart coronary angiography used to be the gold standard. Since CT technology has drastically improved in the past couple of decades cardiac CT has now become the gold standard. Cardiac CT is less invasive and allows the patient to be subjected to less radiation. If a technology that is non invasive and safe, such as EIT, could obtain accurate diagnostic information for the heart and would spare the patient from undergoing cardiac CT it would benefit cardiologists greatly. Therefore, a collaboration with the heart institute began to create a CT vs. EIT study to see what types of cardiac diagnostic information could be acquired by EIT and to what degree of accuracy.

The UOHI has a highly structured and time sensitive CT procedure. First course of action was to observe the CT imaging procedure in order to devise the preliminary EIT imaging procedure that would compliment it and allow for accurate and timely EIT data acquisition of cardiac information. The preliminary experiments were run in order to work out the unforeseen complications that arise during protocol creation. The first experiments tested EIT patient preparation and acquisition times to more

accurately predict frequency of patient EIT imaging and better informed consent. Then several EIT electrode placements were tested to discover which EIT placements would yield more consistent cardiac readings. It was subsequently discovered that the exact physiological location of EIT electrodes on CT scans played an important role in future EIT vs. CT analysis. EIT patient preparation was altered to allow four marker electrodes to be placed on the patient during CT scans. A detailed CT image acquisition procedure and the final EIT acquisition procedure is depicted and described in detail in the following sections.

4.1 Computed Tomography Image Acquisition Procedure (Figure 4.1)

In order to create an EIT image acquisition procedure the CT image acquisition procedure had to be studied. The CT images are acquired with the following procedure at the Ottawa University Heart Institute. First, the patient arrives at the CT imaging department and is greeted by a nurse. The nurse first explains the possible risks and side effects with CT imaging to the patient and the patient signs a consent form. Then the nurse proceeds to take the patient's blood pressure and heart rate. If the blood pressure andor heart rate is too high to acquire CT images the nurse will administer medication (beta blockers) in an attempt to get their vitals in the range to proceed with CT imaging. The nurse then inserts an intravenous needle and places the patient in the CT waiting area.

Once the CT technicians are ready for the patient they are taken to the CT imaging room were the patient is placed on the CT scanner table and the nurse explains the CT imaging procedure (breathing, equipment noise, etc.), places two ECG electrodes in the upper right quadrant of the chest and hooks the patient up to the saline and tracer ejection pump. The first imaging cycle begins with the injection
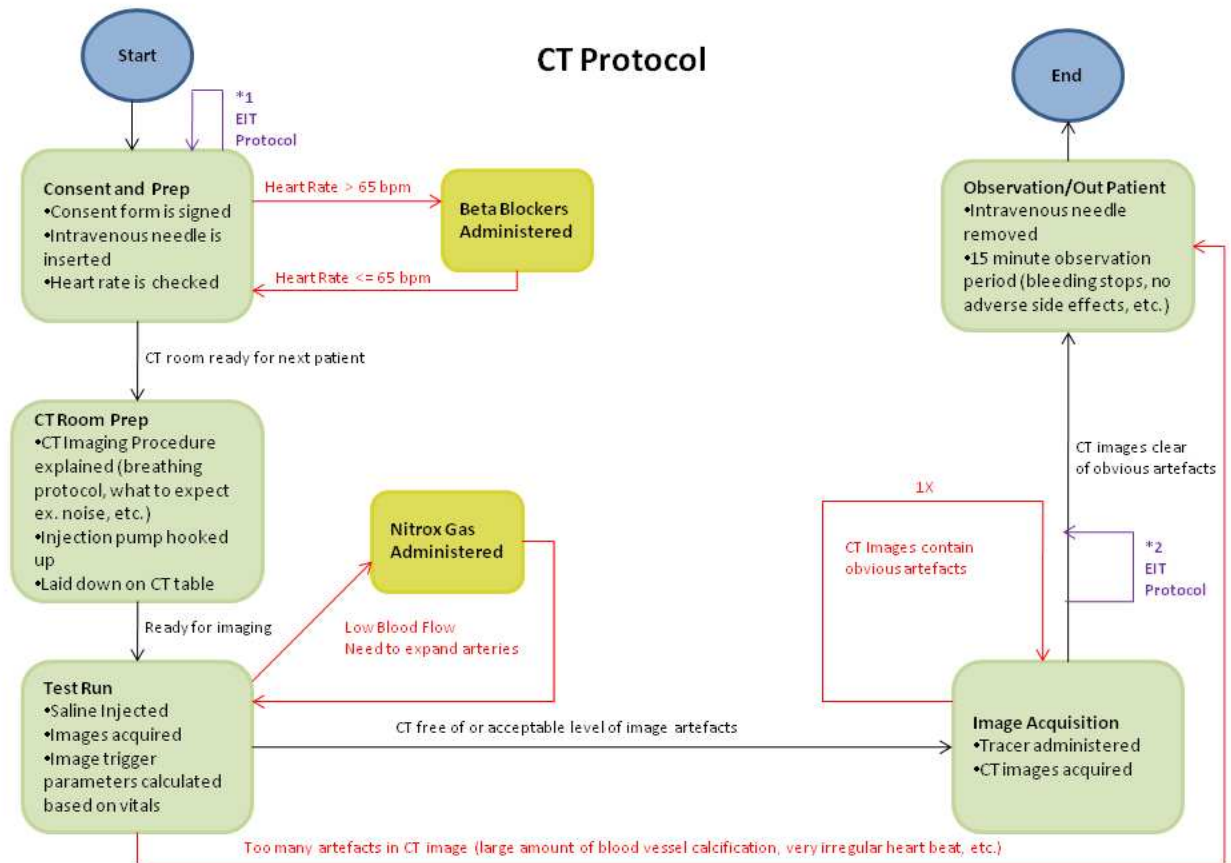
Figure 4.1: CT Protocol

of saline into the patient while the CT scanner runs through an image acquisition cycle. While the patient is being imaged by the CT the following breathing protocol is used: The patient has to breath in for 3 seconds, breath out for 3 seconds, breath in for 3 seconds, breath out for 3 seconds, breath in for 3 seconds and breath hold for 15 seconds. During this first image acquisition cycle the technicians look at the preliminary images and make the required triggering calculations based on the persons heart rate. It is in this cycle that the technicians can spot certain imaging problems like movement artifact, blood vessel calcification, and other imaging problems that would need to be fixed for the final imaging cycle or would prevent the patient from achieving accurate cardiac CT imaging. If there are imaging problems due to lack of blood flow, Nitroglycerin gas is administered by the technician before the second round of imaging in order to open up their blood vessels.

When the patient is ready, the second CT image acquisition cycle begins. This time a tracer is injected into the patient and all the images are saved electronically and sent to the physician for study.

After the second CT scan is taken and everything was found to be sufficiently free of artifacts, the patient is escorted once again to the CT waiting room. A nurse must remove their intravenous needle and the patient will remain for a fifteen minute observation period.

4.2 EIT Image Acquisition Procedure (Figure 4.2)

The Cardiac CT department is always busy and CT scans are expensive and therefore it is important that each scan is done well the first time. That is why the physician and technicians had two requests that had to be followed. First our procedure should not significantly increase their procedure time and second our procedure should not interfere with their procedure or cause any imaging abnormalities.
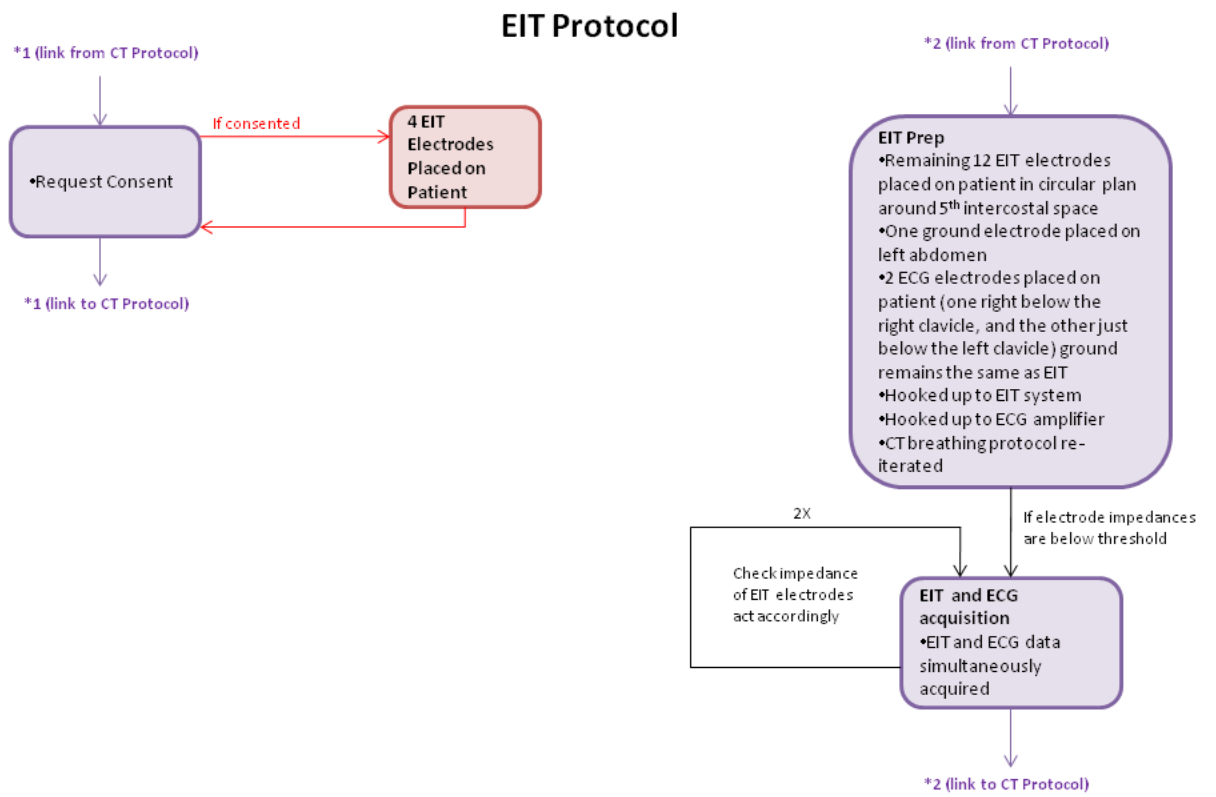
Figure 4.2: EIT Protocol

Since the electrodes we are using for our EIT scan were not X-ray transparent and our equipment is not triggered remotely the EIT imaging could not take place simultaneously with the CT scan at this time. All personnel have to be behind a protective barrier while the CT imaging takes place due to radiation risks and too many non x-ray transparent electrodes could interfere with CT images. Since the scans with the two modalities could not be done simultaneously a procedure had to be created were they could later be aligned through software.

Since the patient has to wait after seeing the nurse and before their CT scan, it was found that this would be the ideal time to recruit them for EIT imaging. During recruitment the approved ethics consent form found in appendix A is handed to the patient and the EIT procedure is explained and they are reminded that they do not have to consent to this procedure.

If the patient consented to undergo EIT imaging following their CT scan, we accompany them into the CT imaging room. Before their CT scan three marker electrodes are placed in the centre and on each side of the patient in line with the 5th intercostal region. The CT technician concluded that up to 4 electrodes could be placed on the patient without any image interference for their purposes. This step would allow us to see were the 16 EIT electrodes would eventually be placed with regards to the CT image. The 5th intercostal region was chosen for the EIT electrode placement since the heart is located between the 4th and 5th intercostal region.

After the CT scan is completed the patient is escorted to an adjacent room were the EIT equipment is set up before hand. They are asked again if they still want to go through with the EIT procedure. Once they reaffirm their consent the remaining 13 electrodes are placed around the 5th intercostal region and a ground electrode is placed on the lower left abdomen region. The two ECG electrodes that remained on the patient following the CT scan are used as well for the EIT scan.

Once all the required 19 electrodes are on the patient. The EIT system is hooked

up to the 16 electrodes and the ground and the ECG amplifier is hooked up to the two ECG electrodes and the PicoScope oscilloscope. Then the patient is instructed to lay down on the provided bed. The CT breathing protocol described in the previous section is described again to the patient since it is used for EIT image acquisition as well. Once the patient is ready ECG and EIT data is acquired simultaneously for a 30 second period of time during the CT breathing protocol. This measurement cycle is repeated two to three times to assure at least one set of good measurements.

Once the EIT information is acquired the electrodes are removed and the patient is escorted to the CT waiting area to have their intravenous needle removed by the nurse and wait for a fifteen minute observations period. The EIT procedure runs between fifteen to twenty minutes. Most of the time is consumed by electrode placement and discussion. The procedure is required to be short since most patients have another procedure following or their blood sugar is low due to the required fasting for CT scanning.

4.3 Summary

Our goal was to create an EIT image acquisition procedure that would not interfere with the existing CT image acquisition procedure in any way and allow us to eventually analyse the images from the two modalities. This goal was achieved by observing the CT protocol and placing our EIT protocol in pockets of CT protocol downtime.

Chapter 5

EIT Image Reconstruction Algorithm

CT data, ECG data, EIT sync pulse, and EIT raw data is collected for each patient using the CT and EIT protocol described earlier. The goal of this chapter is to derive a set of offline software techniques for cardiac EIT image reconstruction. These techniques were divided into seven steps. Several challenges were addressed in order to obtain cardiac EIT images, including finding a method to correlate all the signals, and devising an algorithm in order to properly filter the EIT raw data to focus on the heart information it contains. The following steps were taken to address the challenges: First the ECG data is filtered and the R peak in the QRS signals are detected (steps 1,2,3), second the start and end time is located on the EIT sync pulse (step 4), then the EIT data is filtered and aligned with the EIT sync pulse times (step 5). The ECG R peak times are then located on the EIT data (step 6), and finally a novel method of ensemble averaging is used to achieve a better temporal resolution for heart activity (step 7).

The code to accomplish all of these steps can be found in appendix B.
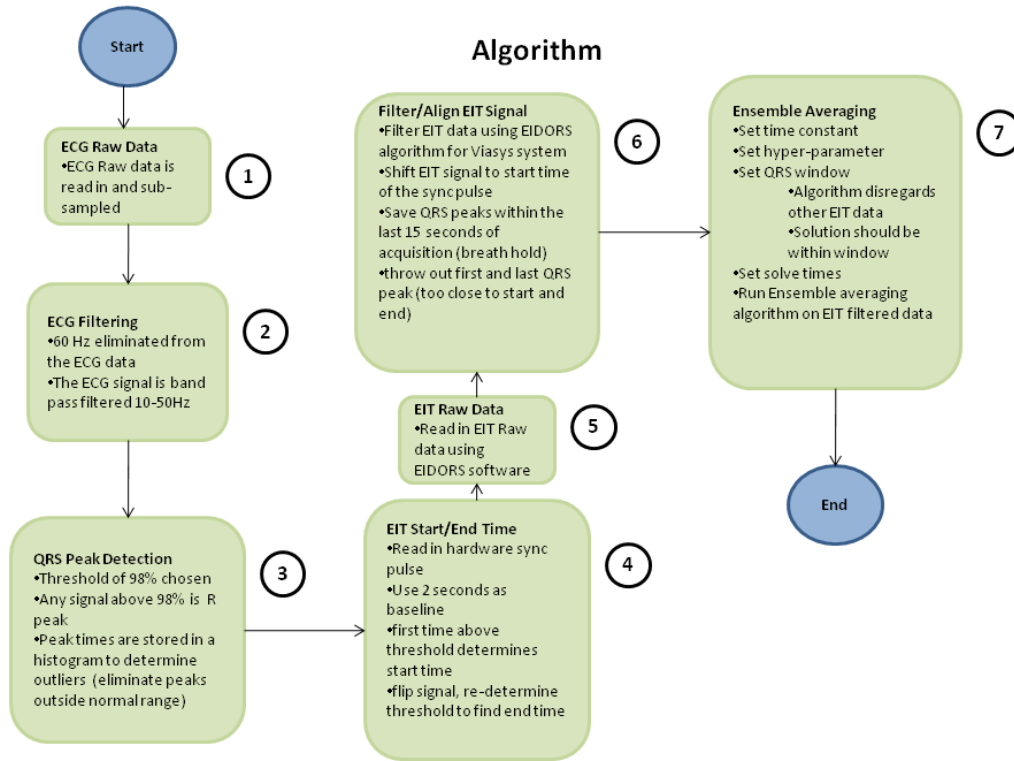
Figure 5.1: The 7 steps of proposed EIT image reconstruction algorithm

5.1 ECG Data Filtering and QRS Peak Detection - Steps 1, 2 and 3

In this section the ECG raw data is processed to filter out the added GOE MF II EIT system noise to obtain accurate peak detection. The three step process can be found in figure 5.1 as steps 1, 2 and 3. In Step 1, the raw ECG data is read and sub-sampled. The ECG signal is sampled at a rate of 50000 samples per second. The ECG signal that is being measured should have a bandwidth of $3Hz$ to $100Hz$ [1]. Therefore, the acquisition rate of our data is greater than is needed. According to the Nyquist theorem a signal acquired can be uniquely reproduced from a signal that is sampled at a rate equal to or greater than twice the maximum frequency component of the original signal [42]. If the Nyquist theorem is not adhered to the

sub-sampled signal cannot be used to uniquely reproduce the original signal due to aliasing [42]. The ECG signal is sub-sampled by a factor of 100, which reduces the 50000 samples per second to 500 samples per second. This $500Hz$ rate exceeds the minimum required $200Hz$ Nyquist criteria. A section of the sub-sampled signal is displayed in figure 5.2 part (a). In order to find the QRS peaks in the ECG data, the ECG signal needs to be filtered to remove any noise. For Step 2 the noise is removed by eliminating $60Hz$ power line component of noise from the signal and all of its harmonics with a first order bandpass filter using a band pass of $10Hz$ to $50Hz$. Components of the PQRST signal such as the P wave fall outside of the lower $10Hz$ range of the bandpass filter. For this step the only region of interest is the R peak of the PQRST wave with a frequency of around $15Hz$ [1]. This frequency falls within the bandpass filter passband of $10Hz$ to $50Hz$ and the R component of the PQRST wave is preserved.
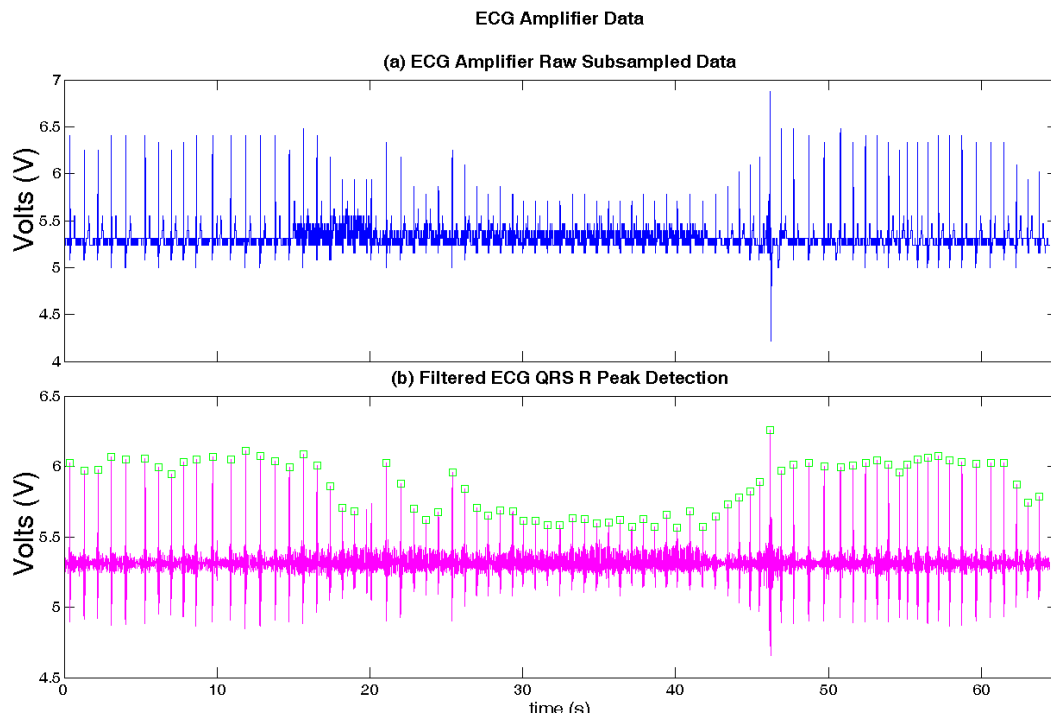
Figure 5.2: ECG Amplifier Data: (a) ECG Raw Sub-sampled Data and (b) ECG Filtered QRS R Peak Determination

Once the signal is filtered the ECG signal is ready for Step 3: processing with a QRS detection algorithm. The ECG signal contains R peaks of different magnitudes. Therefore, choosing a specific voltage threshold that would work for an individual or a group of subjects is difficult. Another way to look at this problem is one can analyse what percentage of the signal is R wave and what percentage is the rest. A percentage threshold can then be chosen to eliminate what is not R wave and peak detection can be achieved. That is why the QRS detection algorithm chosen requires the selection of a threshold which is based on how much of the overall QRS signal is ased to be R signal. A threshold of 98 percent was chosen to represent the part of the signal that was not R wave since it was shown to yield best detection results. This means everything above this threshold (2 percent) is R wave. Since only the peaks of the R wave is of interest, the rest of the ECG signal can be ignored and the ECG signal components below the threshold are eliminated. The R wave portion of the signal is then cycled through to find each maximum (R peak locations). Biological signals are susceptible to large variances due to noise or pre-existing health conditions. For instance, some people might have arrhythmic heart beats creating an opportunity of obtaining false positive peaks. These false positive peaks need to be eliminated since they will cause errors later on in the ensemble averaging algorithm. If the spacing between QRS peaks is above or below a certain threshold the peaks are eliminated from the list to minimise the amount of false positives. This spacing threshold can be determined by using a histogram on the space in between QRS peaks. The result from QRS detection performed on the Raw ECG signal can be seen in figure 5.2 graph (b).

5.2   EIT Acquisition Start and End Determination - Step 4

The purpose of step number 4 is to extract a start and end time from the hardware sync pulse data. The EIT hardware sync pulse signal indicates when EIT measurements began and terminated. This information is useful in order to line up the EIT signal with the ECG signal. The PicoScope sync pulse data is found to have magnitude changes throughout acquisition due to the auto scaling functionality of the scope. This required a more sophisticated algorithm to determine the start and end time than simple edge detection. The sync pulse signal was captured, sub-sampled and the $60Hz$ noise was eliminated with a comb filter. The first two seconds of the signal is chosen as baseline. The mean and standard deviation of this two second interval is determined. The start time is chosen based on when the signal deviates from this two second baseline a specified amount. The end time of the signal is chosen in the same manner as the start time but now the signal and time are flipped and therefore the end of the sync pulse signal becomes the beginning and the same algorithm is run. The result from this step can be seen in figure 5.3 where the sync pulse signal is in red and the start and end time are marked as vertical lines in black colour.

5.3   EIT Data Filtering and Alignment - Step 5 and 6

The final step before Ensemble Averaging is to align the EIT signal to the start and end time found in the step 4 and to locate all the QRS peaks that fall within the breath hold region in the CT breathing protocol. First the EIT signal is read in using the EIDORS open source software. The GOE MF II EIT system used has a known channel artifact which presents itself as a sharp change on a channel of the
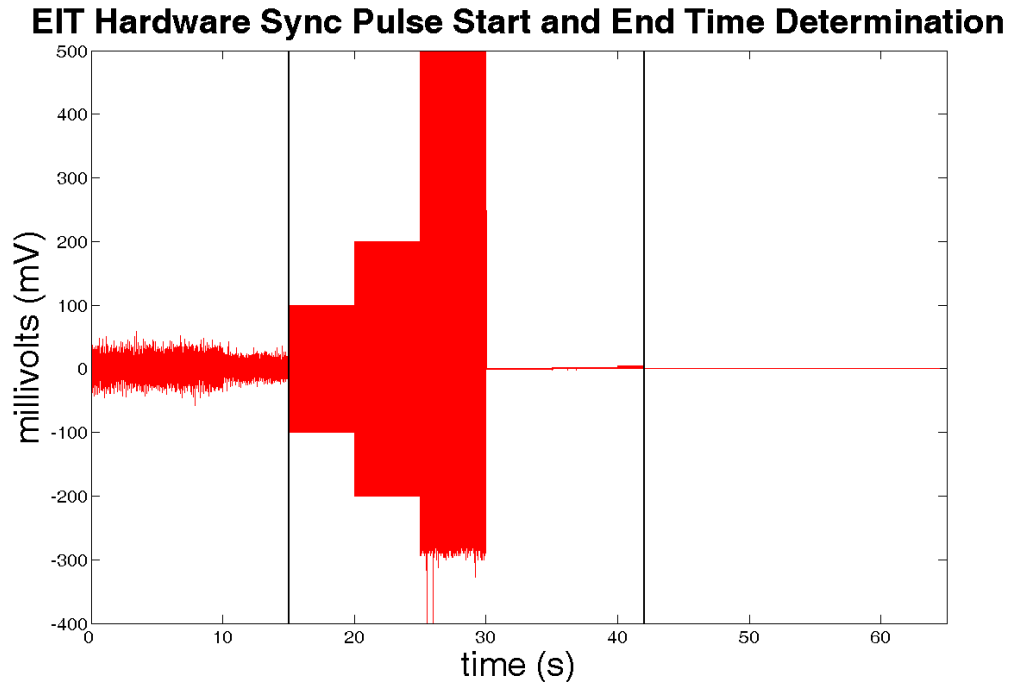
Figure 5.3: EIT Hardware Sync Pulse Start and End Time Determination. Instead of a single step the sync pulse signal is shown as a several step signal due to the auto ranging characteristic of the Picoscope. The Picoscope splits the entire signal into several separate files. The signal is then pieced together from 10 or more separate files each file has a different scaling range.

raw EIT data. The raw EIT signal is checked and filtered for this artifact. The EIT signal is then shifted to the new start that was located by the sync pulse and displayed. Looking at the EIT signal, the time range the breath hold took place can be determined since it's approximately 15 seconds into the EIT protocol. As can be seen in figure 5.4 in the blue EIT signal, the signal goes down for the expiratory breaths and up for the inspiratory breaths before the equilibrium is attained during the breath hold. The ECG QRS peaks are located during this interval, saved, and indicated on figure 5.3 with vertical black lines. QRS peaks that are too close to the
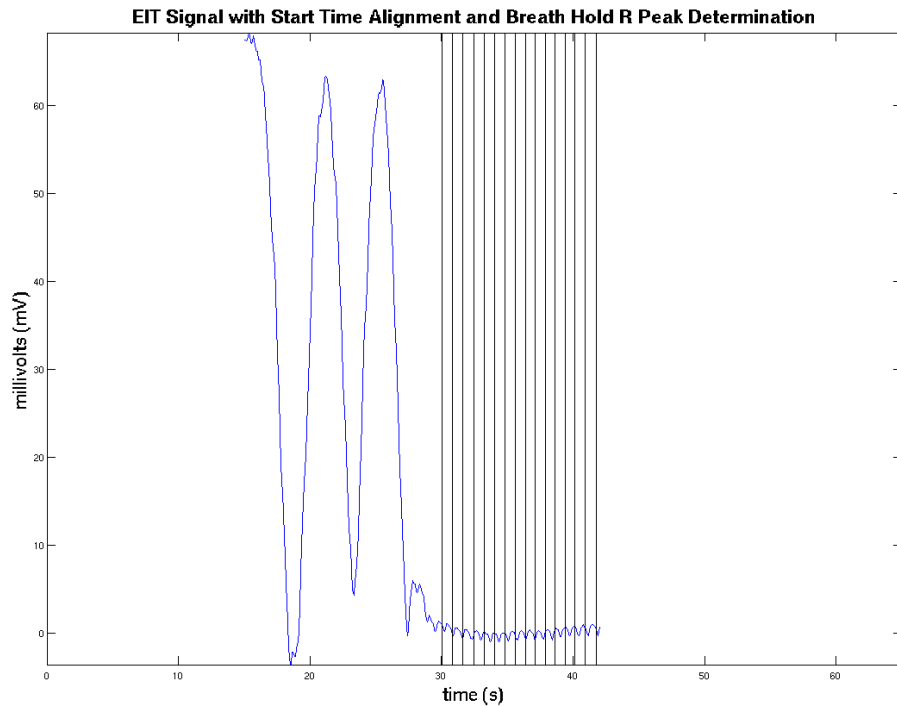
Figure 5.4: Aligned average image with R Peak Determination During Breath Hold

start and end of the breath hold are discarded.

5.4 Ensemble Averaging - Step 7

The goal of step number 7 is to derive a novel ensemble averaging technique that will isolate the cardiac contribution of the EIT signal to produce cardiac EIT images with high temporal resolution. EIT measurements are based upon changes in the body (underlying organs and tissue) [16]. One of the biggest impedance changes is produced when the large organ of the lungs fills with air and then deflates as a person takes an inspiratory and expiratory breath. Cardiac related changes (changes correlated with the cardiac cycle) are caused by blood movement in the heart, which is a relatively small impedance change, and can be difficult to obtain from EIT measurements. Another inherent property of EIT is that its image spatial resolution is low, but EIT

temporal resolution can be high. Since the cardiac frequency components reside in the frequency range of $10 - 25Hz$, good temporal resolution is desired [28].

In order to eliminate the part of the EIT signal that is not correlated with the cardiac signal, and to increase the temporal resolution of the heart information, an ensemble averaging technique has been proposed. This will ensure that only EIT signals that correspond to heart frequencies are used. By solving one inverse problem the heart signal can be determined at all times and a sufficient temporal resolution can be obtained.

This section describes the derivation of a novel ensemble averaging technique. A pictorial description of this technique can be found in figure 5.5. In step 1 and 2 of the figure, simultaneous ECG and EIT data is acquired. In step 3 the EIT and ECG data are aligned and the R peak is located. Then a QRS window time is chosen and all EIT data that does not fall into these time segments are discarded. In step 5 the QRS segments are aligned for use in the ensemble averaging technique. The final algorithm can be found in section 5.4.5 equation 5.25. For step 5 and 6, the matrix form of the solution found in equation 5.25 defines Matrices A,B, and C which are calculated from using the QRS aligned EIT data. Matrices A is populated using time t_w for which the algorithm is solved for.

5.4.1   Methodology

The novel ensemble averaging technique in this thesis is based on a previous temporal one step solver technique devised in Tao Dai's thesis [16]. Both algorithms assume that EIT images are smooth and highly correlated with images in close vicinity in time. The reference one-step solver described in his thesis is uses past and future frames to improve reconstructed image noise. The novel temporal solver algorithm derived in this thesis is based on the same principle that the image is smooth and implements prior space based correlation of elements. This algorithm differs in several ways (one minor, two key differences). The minor difference is that image voxels are
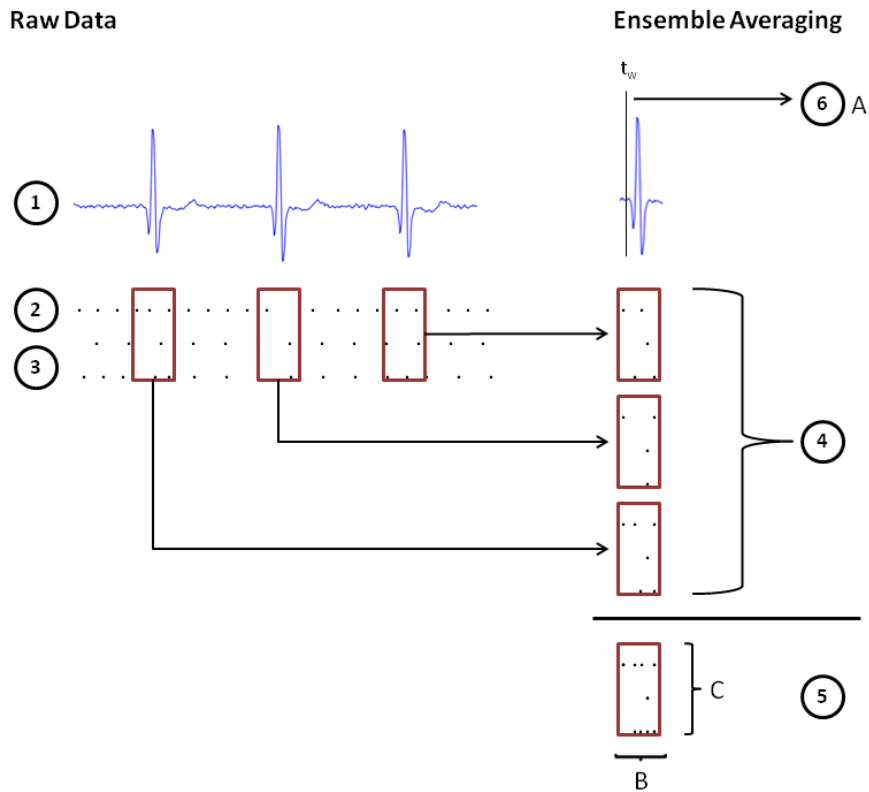
Figure 5.5: Ensemble Averaging: 1. Simultaneous ECG Raw Data is acquired, 2. Simultaneous Raw EIT measurements are acquired, 3. Identify Desired QRS Segments in the EIT raw data and discard the rest, 4. Align the QRS segments of EIT data, 5. Calculate Matrices B and C with QRS segments (equation 5.24), 6. Calculate matrix A for desired solution located at time t_w (equation 5.24)

considered as separable components in space and time. This change reduces the complexity of the algorithm since the inverse problem now only needs to be solved once for every iteration of averaging. This reduction in computational complexity allows this algorithm to run faster between iterations. A key distinguishing feature of the algorithm developed in this thesis is that it is capable of generating a solution for any arbitrary time, including those in which EIT measurements might not have been acquired. Another feature is the comparison algorithm assumes that the values of each frame where taken at the same time, while this algorithm explicitly considers that each value could be taken at a different time.

5.4.2   The Forward Problem

As described in the background the GOE MF II EIT system used in this thesis operates with 16 electrodes (n_e). Stimulation starts between electrode 1 and 2. Electrode 1 is located at front centre of the patient. The other electrodes are receiving (voltages are measured). Electrode pair 2 and 3 are stimulated next. This stimulation and measurement pattern continues in a counter clockwise direction. The resulting voltage measurements from each frame are stored in a vector $\mathbf{v}$. The EIT measurements are difference measurements. The difference EIT vector $\mathbf{y}$ is calculated $[\mathbf{y}]_i = [v_2]_i - [v_1]_i$. These EIT measurements are modelled using a Finite Element Method (FEM) in order to approximate a solution. The FEM is created by distributing the measured conductivities $(\tilde{c} \in \mathbb{R}^{n_N})$ onto n_N number of piecewise smooth elements. Difference EIT utilises the difference in conductivities, therefore, a vector of conductivity changes is given by $\tilde{x} = c_p - c_r$ (where c_p is present conductivity measurement and c_r is the reference conductivity measurement). If the conductivity variation around the reference c_r is small the relationship between $\mathbf{x}$ and $\mathbf{y}$ is linear. This produces the EIT forward solution found in equation 5.1. In the forward problem tilde ($\tilde{}$) over a variable represents the ensemble value of that variable while the lack of tilde over a variable represents actual data with flaws. While, N represents the number of measurements $\mathbf{y}_i$ ($\mathbf{y}$ representing the actual image) at time t_i. It is desired to estimate the difference image $\mathbf{x}_0$ at time $t_w = t_0$ even though measurements might not have been made at time t_0 that is why the first column of Jacobian matrix $\mathbf{J}$ is zero. The Jacobian matrix also referred to as the sensitivity matrix in equation 5.1 is a matrix comprised of partial derivatives voltage with respect to conductivity [19] computed from the FEM. Variable $\mathbf{n}$ represents white Gaussian noise.

$$\begin{bmatrix} \mathbf{y}_1 \\ \mathbf{y}_2 \\ \vdots \\ \mathbf{y}_N \end{bmatrix} = \begin{bmatrix} 0 & \mathbf{J}_1 & \cdots & 0 \\ \vdots & \vdots & \cdots & \vdots \\ \vdots & \vdots & \cdots & \vdots \\ 0 & 0 & \cdots & \mathbf{J}_N \end{bmatrix} \begin{bmatrix} \mathbf{x}_0 \\ \mathbf{x}_1 \\ \vdots \\ \mathbf{x}_N \end{bmatrix} + \begin{bmatrix} \mathbf{n}_0 \\ \mathbf{n}_1 \\ \vdots \\ \mathbf{n}_N \end{bmatrix} \tag{5.1}$$

and also as

$$\tilde{\mathbf{y}} = \tilde{\mathbf{J}}\tilde{\mathbf{x}} + \tilde{\mathbf{n}} \tag{5.2}$$

5.4.3   The Inverse Problem and Regularisation

The EIT forward problem represents an "ill posed" problem. In order to solve an ill posed problem a method of regularisation is required [19]. Electricity in the body can take many different paths which makes EIT imaging so difficult. In order to reconstruct an image one must predict what the most likely scenario was to cause the measurements at each electrode. In order to make this prediction the following question needs to be answered. Given actual image $\tilde{\mathbf{y}}$ what is the difference image $\tilde{\mathbf{x}}$ that most likely caused $\mathbf{y}$? Bayes' theorem is used in statistics to calculate the relationship between conditional probabilities of random variables [35]. $P(\tilde{\mathbf{x}}|\tilde{\mathbf{y}})$ represents the notation for probability of difference image $\tilde{\mathbf{x}}$ given $\tilde{\mathbf{y}}$ [35]. The derivation of Bayes' Theorem is found in equations 5.3 [35]. Where, $P(\tilde{\mathbf{x}}, \tilde{\mathbf{y}})$ is the probability of $\tilde{\mathbf{x}}$ and $\tilde{\mathbf{y}}$ [27] [35]. $P(\tilde{\mathbf{x}}|\tilde{\mathbf{y}})$ is the conditional probability of difference image $\tilde{\mathbf{x}}$ occurring given actual image $\tilde{\mathbf{y}}$ [35]. $P(\tilde{\mathbf{y}})$ is the probability of actual image $\tilde{\mathbf{y}}$ [35].

$$P\left(\tilde{\mathbf{x}}, \tilde{\mathbf{y}}\right) = P\left(\tilde{\mathbf{x}}|\tilde{\mathbf{y}}\right) P\left(\tilde{\mathbf{y}}\right) = P\left(\tilde{\mathbf{y}}|\tilde{\mathbf{x}}\right) P\left(\tilde{\mathbf{x}}\right) \tag{5.3}$$

$$P\left(\tilde{\mathbf{x}}|\tilde{\mathbf{y}}\right) = \frac{P\left(\tilde{\mathbf{y}}|\tilde{\mathbf{x}}\right) P\left(\tilde{\mathbf{x}}\right)}{P\left(\tilde{\mathbf{y}}\right)} \tag{5.4}$$

Suppose that variable $\tilde{\mathbf{x}}$ is an independent multivariate Gaussian with noise $\tilde{\mathbf{n}}$. The

expected image covariance of $\tilde{\mathbf{x}}$ is $\mathbf{\Sigma}_{\tilde{x}} \in \mathbb{R}^{n_N \times n_N}$ and the mean is $\bar{\mathbf{x}}$. $\mathbf{\Sigma}_{\tilde{n}} \in \mathbb{R}^{n_M \times n_M}$ is the covariance matrix of the noise $\tilde{\mathbf{n}}$ with zero mean. The noise measurement $\tilde{\mathbf{n}}$ is uncorrelated because each noise measurement is made independently and each channel has the same noise. Then $\mathbf{\Sigma}_{\tilde{n}}$ is a diagonal matrix with $[\mathbf{\Sigma}_{\tilde{n}}]_{i,i} = \sigma_i^2 I$, where σ_i^2 is the noise variance at measurement i and $\mathbf{I}$ is the identity matrix. Given these parameters the distribution of the image can be modelled as $P(\tilde{x})$ in equation 5.5.

$$P(\tilde{\mathbf{x}}) = \frac{1}{(2\pi)^{\frac{N}{2}} \sqrt{|\Sigma_{\tilde{\mathbf{x}}}|}} e^{-\frac{1}{2}(\tilde{\mathbf{x}} - \bar{\mathbf{x}})^t \Sigma_{\tilde{\mathbf{x}}}^{-1}(\tilde{\mathbf{x}} - \bar{\mathbf{x}})} \tag{5.5}$$

The a posteriori distribution of $\tilde{y}$ given conductivity distribution of $\tilde{x}$ can be written as equation 5.6.

$$P(\tilde{\mathbf{y}}|\tilde{\mathbf{x}}) = \frac{1}{(2\pi)^{\frac{M}{2}} \sqrt{|\Sigma_{\tilde{\mathbf{n}}}|}} e^{-\frac{1}{2}\left(\tilde{\mathbf{y}} - \tilde{\mathbf{J}}\tilde{\mathbf{x}}\right)^t \Sigma_{\tilde{\mathbf{n}}}^{-1}\left(\tilde{\mathbf{y}} - \tilde{\mathbf{J}}\tilde{\mathbf{x}}\right)} \tag{5.6}$$

Bayes Theorem can now be re-written as equation 5.7.

$$P(\tilde{\mathbf{x}}|\tilde{\mathbf{y}}) = \frac{e^{-\frac{1}{2}\left[\left(\tilde{\mathbf{y}} - \tilde{\mathbf{J}}\tilde{\mathbf{x}}\right)^t \Sigma_{\tilde{\mathbf{n}}}^{-1}\left(\tilde{\mathbf{y}} - \tilde{\mathbf{J}}\tilde{\mathbf{x}}\right) + (\tilde{\mathbf{x}} - \bar{\mathbf{x}})^t \Sigma_{\tilde{\mathbf{x}}}^{-1}(\tilde{\mathbf{x}} - \bar{\mathbf{x}})\right]}}{(2\pi)^{\frac{M+N}{2}} \sqrt{|\Sigma_{\tilde{\mathbf{x}}}| |\Sigma_{\tilde{\mathbf{n}}}|} P(\tilde{\mathbf{y}})} \tag{5.7}$$

To obtain the most likely difference image $\tilde{\mathbf{x}}$ given actual image $\tilde{\mathbf{y}}$ a Maximum A Posteriori (MAP) estimation method is used. This method of regularisation is used to derive a point estimate of a quantity based on empirical information obtained [41]. The MAP estimation is a good method to use to obtain the inverse solution to this question. The MAP estimate $(\hat{x}_{MAP})$ is found by maximising the a posteriori probability $P(\tilde{\mathbf{x}}|\tilde{\mathbf{y}})$ in equation 5.7. Minimising the exponent (equation 5.8) maximises the a posteriori from the previous equation.

$$\hat{\mathbf{x}}_{MAP} = arg\ min_{\tilde{\mathbf{x}}} \left| \left(\tilde{\mathbf{y}} - \tilde{\mathbf{J}}\tilde{\mathbf{x}}\right)^t \Sigma_{\tilde{\mathbf{x}}}^{-1} \left(\tilde{\mathbf{y}} - \tilde{\mathbf{J}}\tilde{\mathbf{x}}\right) + (\tilde{\mathbf{x}} - \bar{\mathbf{x}})^t \Sigma_{\tilde{\mathbf{n}}}^{-1} (\tilde{\mathbf{x}} - \bar{\mathbf{x}}) \right| \tag{5.8}$$

This yields the MAP estimate found in equation 5.9.

$$\hat{\mathbf{x}}_{MAP} = \left(\tilde{\mathbf{J}}^t \Sigma_{\tilde{\mathbf{n}}}^{-1} \tilde{\mathbf{J}} + \Sigma_{\tilde{\mathbf{x}}}^{-1}\right)^{-1} + \left(\tilde{\mathbf{J}}^t \Sigma_{\tilde{\mathbf{n}}}^{-1} \tilde{\mathbf{y}} + \Sigma_{\tilde{\mathbf{x}}}^{-1} \bar{\mathbf{x}}\right) \tag{5.9}$$

The MAP estimate can be re-written as equation 5.10.

$$||\tilde{\mathbf{y}} - \tilde{\mathbf{J}}\tilde{\mathbf{x}}||^2_{\Sigma_{\tilde{\mathbf{n}}}^{-1}} + ||\tilde{\mathbf{x}} - \bar{\mathbf{x}}||^2_{\Sigma_{\tilde{\mathbf{x}}}^{-1}} \tag{5.10}$$

5.4.4   One Step Gaussian Solver and NOSER Algorithm

A one step Gaussian Solver is implemented to take the inverse problem in equation 5.10 and represent it as a linear reconstruction matrix which can be easily solved by a computer [12]. Minimising the error in equation 5.10 we obtain the one step linearised inverse in equation 5.11. Measurement accuracy $\mathbf{W} = \sigma_{\tilde{n}}^2 \Sigma_{\tilde{n}}^{-1} = \mathbf{I}$ and regularisation matrix $\mathbf{R} = \sigma_{\tilde{x}}^2 \Sigma_{\tilde{x}}^{-1}$ are defined to calculate $\sigma_{\tilde{n}}$ and $\sigma_{\tilde{x}}$ respectively. Variable σ_n is the average measurement noise amplitude and $\sigma_{\tilde{x}}$ represents the *a priori* amplitude of conductivity change. A regularisation hyper parameter λ is used to control the trade off between resolution and noise attenuation. The hyper parameter is defined in equation 5.12 to obtain equation 5.13.

$$\tilde{\mathbf{x}}_{est} = \left(\tilde{\mathbf{J}}^t \frac{1}{\sigma_n^2} \mathbf{W} \tilde{\mathbf{J}} + \frac{1}{\sigma_x^2} \mathbf{R}\right)^{-1} \tilde{\mathbf{J}}^t \frac{1}{\sigma_n^2} \mathbf{W} \mathbf{y} \tag{5.11}$$

$$\lambda = \sigma_n / \sigma_x \tag{5.12}$$

$$\tilde{\mathbf{x}}_{est} = \left(\tilde{\mathbf{J}}^t \mathbf{W} \tilde{\mathbf{J}} + \lambda^2 \mathbf{R}\right)^{-1} \tilde{\mathbf{J}}^t \mathbf{W} \mathbf{y} = \mathbf{B} \mathbf{y} \tag{5.13}$$

Matrix $\mathbf{B}$ in equation 5.14 is the linear one step inverse of equation 5.13.

$$\mathbf{B} = \left(\tilde{\mathbf{J}}^t\mathbf{W}\tilde{\mathbf{J}} + \lambda^2\mathbf{R}\right)^{-1}\tilde{\mathbf{J}}^t\mathbf{W} \tag{5.14}$$

For independent image elements the regularisation matrix $\mathbf{R}$ turns into the identity matrix $\mathbf{I}$ and zeroth-order Tikhonov regularisation is used. One drawback of the Tikhonov regularisation (with the identity matrix) in EIT is that the noise is pushed to the boundary of the image [19]. This phenomena can be controlled by a scaling factor s. This penalty is used to scale all elements in the regularisation matrix $\mathbf{R}$. For example diagonal element i, i in regularisation matrix $\mathbf{R}$ is represented by $[\mathbf{R}]_{i,i} = [\mathbf{J}^t\mathbf{J}]_{i,i}^s$. When the sensitivity exponent s is 0 the noise is pushed to the boundary of the image while when it is 1 the noise is pushed to the centre of the image. We chose to calculate matrix $\mathbf{R}$ with $s = 0.5$ [12] which allows for an easy inversion of matrix $\mathbf{R}$ and a good compromise between pushing the noise towards the boundary or centre.

In order to put equation 5.13 in Wiener filter form the following substitutions are made: $\mathbf{P} = \mathbf{R}^{-1} = \frac{1}{\sigma_{\tilde{x}}^2}\mathbf{\Sigma}_{\tilde{x}}$ and $\mathbf{V} = \mathbf{W}^{-1} = \frac{1}{\sigma_{\tilde{n}}^2}\mathbf{\Sigma}_{\tilde{n}}$. Equation 5.15 is the solution in Wiener Filter Form and equation 5.16 shows the simplified one step inverse solution.

$$= \left(\tilde{\mathbf{J}}^t\mathbf{W}\tilde{\mathbf{J}} + \lambda^2\mathbf{R}\right)^{-1}\tilde{\mathbf{J}}^t\mathbf{W}\left[\left(\mathbf{J}\frac{1}{\lambda^2}\mathbf{P}\tilde{\mathbf{J}}^t + \mathbf{V}\right)\left(\tilde{\mathbf{J}}\frac{1}{\lambda^2}\mathbf{P}\tilde{\mathbf{J}}^t + \mathbf{V}\right)^{-1}\right]$$

$$= \left(\tilde{\mathbf{J}}^t\mathbf{W}\tilde{\mathbf{J}} + \lambda^2\mathbf{R}\right)^{-1}\left(\tilde{\mathbf{J}}^t\mathbf{W}\tilde{\mathbf{J}} + \lambda^2\mathbf{R}\right)\left(\frac{1}{\lambda^2}\mathbf{P}\tilde{\mathbf{J}}^t\right)\left(\tilde{\mathbf{J}}\frac{1}{\lambda^2}\mathbf{P}\tilde{\mathbf{J}}^t + \mathbf{V}\right)^{-1}$$

$$= \mathbf{P}\tilde{\mathbf{J}}^t\left(\tilde{\mathbf{J}}\mathbf{P}\tilde{\mathbf{J}}^t + \lambda^2\mathbf{V}\right)^{-1} \tag{5.15}$$

$$\tilde{\mathbf{x}}_{est} = \mathbf{\Sigma}_{\tilde{x}}\tilde{\mathbf{J}}^t\left(\tilde{\mathbf{J}}\mathbf{\Sigma}_{\tilde{x}}\tilde{\mathbf{J}}^t + \mathbf{\Sigma}_{\tilde{n}}\right)^{-1}\tilde{\mathbf{y}} \tag{5.16}$$

Legend

N_t number of frames between i,j
N_x number of voxels between i,j
i voxel i
j voxel j
Δt time interval between i,j
Δr distance between i,j
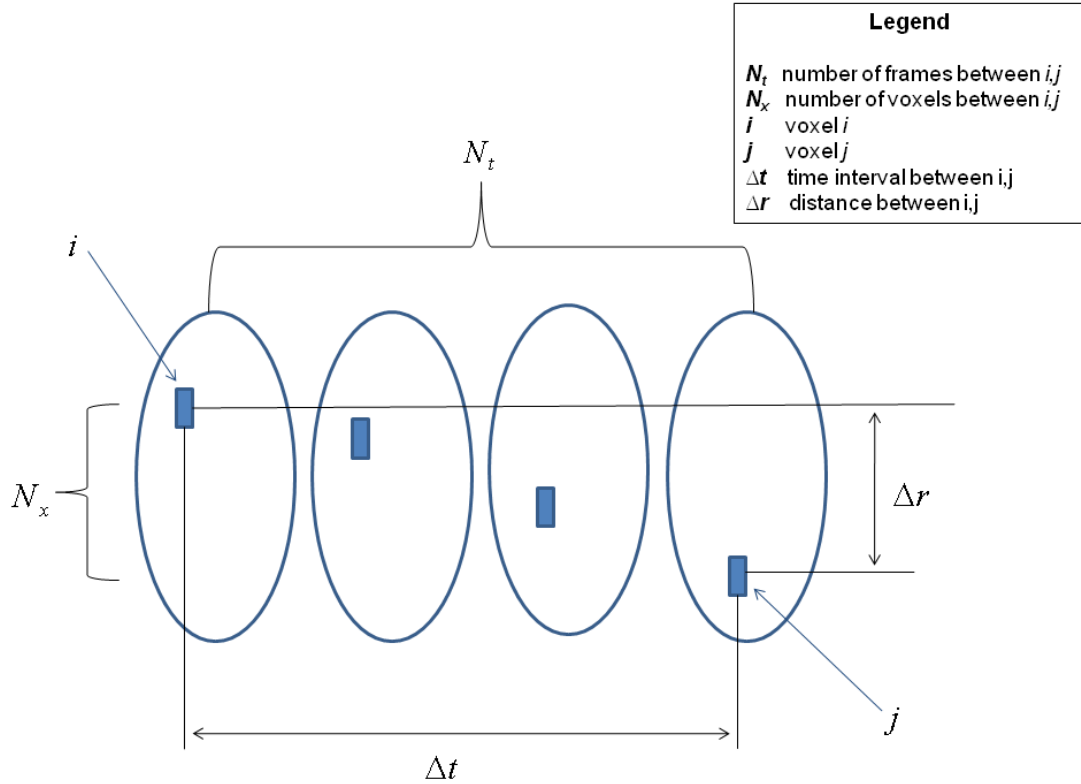
Figure 5.6: Covariance between voxels (i,j)

5.4.5   Temporal Solver

In this section we devise a temporal image reconstruction solver. The goal is to solve all times by solving the solution for one period of time. To accomplish this, prior space based correlation of elements will be implemented and the previously stated inverse problem will include spatial and temporal aspect. When looking at the correlation of frames that are nearby and assuming the image is smooth the closer a frame is to the other the greater the correlation. Frames that are far can be viewed as independent and their correlation is low.

Figure 5.6 depicts voxel i and j and their relationship in space and time. The covariance of voxel i and j is shown in equation 5.17. The space component $\Delta \mathbf{r}$ (difference between $\mathbf{x},\mathbf{y}$ for voxel i,j) and the time component Δt (change in time)

Legend and Substitutions

N_t number of frames between voxel l,j
N_x number of voxels between voxel l,j
$\Sigma_x = \Lambda$
$\gamma = e^{-k2}$
$e^{-k2|ti-tj|} = \gamma_{i,j}$

On the matrix diagonal t_1-$t_1 = \Delta t = 0$

$N_t N_x$

The equation is separable.
Time and spatial
component can be
separated.

$\Lambda e^{-k_2|\Delta t|} = \Lambda \gamma_{i,j}$

Figure 5.7: Covariance matrix explained

are separable since they are in different space and time as shown in equation 5.18. Figure 5.7 depicts the creation of the covariance matrix for voxel i,j. As seen in figure 5.7 $\Sigma_{\tilde{x}} = \Lambda$ on diagonal since $t_1 - t_1 = 0$ therefore $\Delta t = 0$. The following syntax will be used from hence forth: $e^{-k_2|t_i-t_j|} = \gamma^{|i-j|} = \gamma_{i,j}$.

Using covariance the one step Gaussian inverse solution in equation 5.19 will be split up into part p1 and p2 for derivation of the temporal matrix solution.

$$\left[\sum_{\tilde{x}} \right]_{i,j} = e^{-[k_1|\Delta r| + k_2|\Delta t|]} \tag{5.17}$$

$$\left[\mathbf{\Sigma}_{\tilde{x}}\right]_{i,j} = \left[time\right]\left[space\right]$$

$$\left[\mathbf{\Sigma}_{\tilde{x}}\right]_{i,j} = \left[e^{-k_2|\Delta t|}\right]\left[e^{-k_1|\Delta r|}\right] \quad (5.18)$$

$$\tilde{\mathbf{x}}_{est} = \underbrace{\mathbf{\Sigma}_{\tilde{\mathbf{x}}}\tilde{\mathbf{J}}^t}_{p1}\underbrace{\left(\tilde{\mathbf{J}}\mathbf{\Sigma}_{\tilde{\mathbf{x}}}\tilde{\mathbf{J}}^t + \mathbf{\Sigma}_{\tilde{\mathbf{n}}}\right)^{-1}\tilde{\mathbf{y}}}_{p2} \quad (5.19)$$

The covariance equation 5.19 is multiplied and can be split into two parts $p1$ and $p2$. Covariance equation 5.19 can be put into matrix format to derive the matrix solution of the temporal solver.

The matrix solution for part $p1$ is derived in equation 5.20, where the expected image covariance matrix is multiplied with the Jacobian voltage distribution. The ensemble averaging technique solves for one instant in time for every iteration. In this derivation we are solving the solution $x_{0,est}$ for time $t_w = 0$. Therefore, all solutions $x_1...x_N$ at times different from $t_w = 0$ can be discarded. This step results in equation 5.21.

$$\begin{bmatrix} x_0 \\ x_1 \\ \vdots \\ x_N \end{bmatrix}_{est} = \begin{bmatrix} \Lambda & \Lambda_{\gamma_{0,1}} & \cdots & \Lambda_{\gamma_{0,N}} \\ \Lambda_{\gamma_{1,0}} & \Lambda & \cdots & \Lambda_{\gamma_{1,N}} \\ \vdots & \vdots & \ddots & \vdots \\ \Lambda_{\gamma_{N,0}} & \Lambda_{\gamma_{N,1}} & \cdots & \Lambda \end{bmatrix} \begin{bmatrix} 0 & 0 \\ J_1 & 0 \\ \vdots & \vdots \\ 0 & J_N^t \end{bmatrix} \quad (5.20)$$

$$x_{0,est} = \begin{bmatrix} \Lambda_{\gamma_{0,1}}J_1^t & \cdots & \Lambda_{\gamma_{0,N}}J_N^t \end{bmatrix} \quad (5.21)$$

In part p2 of the expected image covariance matrix is multiplied with the Jacobian distribution to derive the matrix in equation 5.22. Next covariance noise is added to the product found in equation 5.22 to arrive at the matrix solution or part2 found in

equation equation 5.23.

$$\tilde{J}\Sigma_{\tilde{x}}\tilde{J}^t = \begin{bmatrix} 0 & J_1 & \cdots & 0 \\ \vdots & \vdots & \ddots & \vdots \\ \vdots & \vdots & \ddots & \vdots \\ 0 & 0 & \cdots & J_N \end{bmatrix} \begin{bmatrix} \Lambda_{\gamma_{0,1}} J_1^t & \cdots & \cdots & \Lambda_{\gamma_{0,N}} J_N^t \\ \Lambda_{\gamma_{1,1}} J_1^t & \cdots & \cdots & \Lambda_{\gamma_{1,N}} J_N^t \\ \vdots & \cdots & \cdots & \vdots \\ \Lambda_{\gamma_{N,1}} J_1^t & \cdots & \cdots & \Lambda_{\gamma_{N,N}} J_N^t \end{bmatrix}$$

$$= \underbrace{\begin{bmatrix} J_1\Lambda_{\gamma_{1,1}} J_1^t & \cdots & \cdots & J_1\Lambda_{\gamma_{1,N}} J_N^t \\ \vdots & \cdots & \cdots & \vdots \\ \vdots & \cdots & \cdots & \vdots \\ J_N\Lambda_{\gamma_{N,1}} J_1^t & \cdots & \cdots & J_N\Lambda_{\gamma_{N,N}} J_N^t \end{bmatrix}}_{NbyNmatrix \quad i,j=J_i\Lambda_{\gamma_{i,j}} J_i^t} \tag{5.22}$$

$$\tilde{J}\Sigma_{\tilde{x}}\tilde{J}^t + \Sigma_{\tilde{n}} = \begin{bmatrix} J_1\Lambda_{\gamma_{1,1}} J_1^t & \cdots & \cdots & J_1\Lambda_{\gamma_{1,N}} J_N^t \\ \vdots & \cdots & \cdots & \vdots \\ \vdots & \cdots & \cdots & \vdots \\ J_N\Lambda_{\gamma_{N,1}} J_1^t & \cdots & \cdots & J_N\Lambda_{\gamma_{N,N}} J_N^t \end{bmatrix} + \begin{bmatrix} \delta_N^2 & 0 & \cdots & 0 \\ 0 & \delta_N^2 & \cdots & 0 \\ \vdots & \vdots & \ddots & \vdots \\ 0 & 0 & 0 & \delta_N^2 \end{bmatrix} \tag{5.23}$$

Where $\tilde{J}\Sigma_{\tilde{x}}\tilde{J}^t + \Sigma_{\tilde{n}} = \begin{cases} J_i\Lambda J_j^t + \delta^2 & when \quad i = j \quad\quad on \quad diagonal \\ J_i\Lambda_{\gamma_{i,j}} J_j^t & when \quad i \neq j \quad\quad off \quad diagonal \end{cases}$

Finally, we are left with the solution in equation 5.24 depicts part p1 and part p2 put back together for the proposed temporal solver algorithm and equation 5.25 its matrix form. This algorithm can predict difference image $\mathbf{x}_{t_w,est}$ for any time t_w. Part p1 represents matrix $\mathbf{A}$, part p2 represents matrix $\mathbf{B}$ and $\tilde{\mathbf{y}}$ represents matrix $\mathbf{C}$ from depiction of the ensemble averaging method in figure 5.5.

$$x_{0,est} = \underbrace{\left[\Sigma_{\tilde{x}} \tilde{J}^t \right]_{top}} _{A} \underbrace{\left(\tilde{J} \Sigma_{\tilde{x}} \tilde{J}^t + \Sigma_{\tilde{n}} \right)^{-1}}_{B} \underbrace{\tilde{y}}_{C} \tag{5.24}$$

$$\begin{bmatrix} M \\ by \\ 1 \end{bmatrix} = \underbrace{\begin{bmatrix} M & by & N \end{bmatrix}}_{A} \underbrace{\begin{bmatrix} N & by & N \end{bmatrix}}_{B} \underbrace{\begin{bmatrix} 1 \\ by \\ N \end{bmatrix}}_{C} \tag{5.25}$$

We can use this temporal solver to ensemble average for as many solutions in time as we would like. Each iteration through the algorithm is derived for a time t_w. Matrix **A** is the only matrix that is calculated only for time t_w. Therefore, matrix **B** and **C** are not effected for each solution after the first iteration. The fact that matrix **B** and **C** are only solved for the first iteration makes this algorithm less computationally expensive which improves the speed of the algorithm. For example, in a scenario where 208 measurements are taken per frame at a frame rate of 13 frames per second for a total of 15 seconds, matrix **B** will hold over $40K$ by $40K$ timing elements which have to be inverted.

5.5 Summary

This chapter described the software and mathematical algorithm portion of the proposed EIT reconstruction algorithm for this thesis. The raw EIT and ECG data is manipulated and filtered to eliminate unwanted noise such as $60Hz$, EIT hardware interference, and lung data. This filtered data is fed into the proposed ensemble averaging algorithm. The ensemble averaging technique can solve for any arbitrary time which leads to greater temporal resolution. The final result from the ensemble averaging algorithm produces a temporal cycle of EIT images. These images depict

blood flow through the patients heart for a duration of a QRS segment.

Chapter 6

Experiments

6.1 Experiments

This chapter presents software simulation and human experiments which were performed to test limitations and validity of the algorithmic framework derived in the previous chapter.

The goal of the software simulation is to use a known signal to analyse the behaviour of the mathematical model. Only the controlled manipulation of random Gaussian noise, hyperperameter value and time constant will affect the behaviour of the mathematical model and image reconstruction. Actual EIT data contains noise and error from several sources such as 60Hz power, instrumentation noise, environment noise (interaction from other systems), random noise, and electrode movement artifacts. If one studies the actual EIT data without the simulation as a control case there is no way of distinguishing what behaviour is caused by the mathematical model and what is caused by error in the data and reconstruction methods.

Human trials is the next step after simulation test cases show desired reconstruction behaviour such as better reconstruction accuracy of the target with added Gaussian noise than naive reconstruction. This step will test the entire cardiac EIT

tool set including the temporal ensemble averaging algorithm. Patient EIT images contain a large lung contribution since inhalation and exhalation produce a large conductivity change in the chest. The cardiac signal is much smaller than the large lung contribution. Different experimental methods and mathematical algorithms need to be used to isolate cardiac portion of the EIT image and filter out the lung contribution. A qualitative analysis will be performed on the resulting EIT images from the human experiments to determine if the algorithm isolates the cardiac EIT data and rejects the rest.

6.2 Software Simulation Model Experiments

Simulations were performed in order to determine reasonable parameters and to identify limitations of the theoretical model. The simulations also serve as a control for comparison against human experimental results.

6.2.1 Software Simulation Model Description

In this software simulation, the thorax of the person is modelled as a 2D finite element model mesh shown in figure 6.1. The heart is modelled as a circular target moving in a clockwise direction inside of this mesh at a certain defined rate (frames per revolution). The target is shown as a blue circle in figure 6.1. The simulation keeps track of the interpolated mesh elements that are selected to represent the target as the target moves. 208 homogenous voltage measurements are taken for each frame by the simulated 14 dark green receiving electrodes. The pair of light green electrodes represent the stimulating electrodes. As the target moves the contrast value (degree of conductivity change) of the underlying mesh changes to match target movement. The simulation requires three parameter inputs which are: frames per revolution, signal to noise ratio, and number of frames. The frames variable (f) stipulates the total number of frames that will be simulated. The time constant (τ) represents the
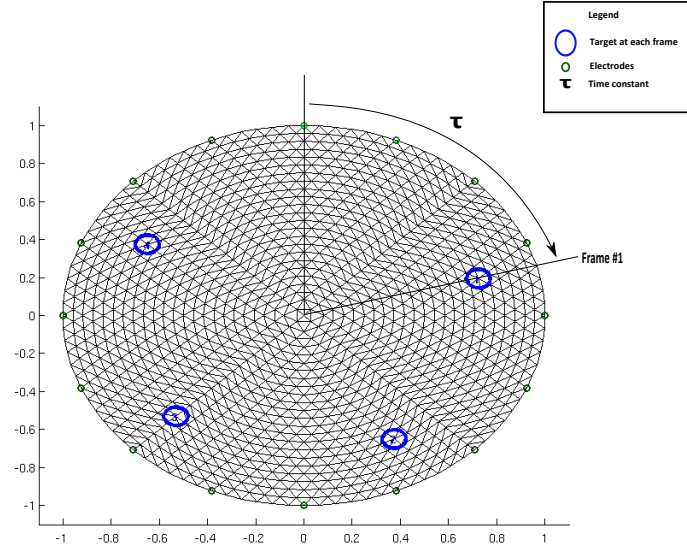
Figure 6.1: Graphical depiction of software simulation. The finite element mesh represents the thorax of the person. The blue circles with numbers represent area on the mesh designated to the target (heart). Each numbered blue circle represents the target in one frame. In this example the target was moving at a speed of 4.8 frames per revolution in a clockwise direction starting from top of circle. τ represents the time constant which is calculated to be 75 degrees for this example. Image was derived using EIDORS software.

degree of revolution per frame. For example if the frames per revolution is equal to 4.8 frames/revolution then $\tau = \frac{1}{4.8 \ frames/rev} \times 360° = 75° \ of \ rev/frame$. In the simulation, 208 measurements were taken during each frame.

The desired white Gaussian noise is added to the signal for each trial in order to see how well the mathematical algorithm can filter resolve an image with this noise level. The signal to noise ratio (SNR) represents the amount of signal vs. noise is present for each measured voltage signal. A larger SNR value represents a decrease in the amount of noise that is added to the simulated EIT signal. The target should be reconstructed clearly even after the addition of white Gaussian noise if the parameters (hyperparameter, time constant) are set properly in the mathematical algorithm. In the simulation several SNR values were used in order to view how well the proposed ensemble averaging technique handles noise. Each level of SNR was derived with the same random seed value allowing for the same mean Gaussian noise distribution

between test cases. The signal with noise is passed to the ensemble averaging technique with varying time constants and hyperparameter values to visualise the effects of these parameters and to aid in parameter selection in human testing.

6.2.2   Simulation Results

For all simulations the revolutions per frame rate was set as 10 and the simulations were run for 100 frames each. EIDORS software was used for the simulations. The mesh model that was used to create simulation is seen in figure 6.1. The model uses 2D square mesh rotated by 45 degrees containing $40x40x2 = 3200$ mesh elements.

Table 6.1 shows results derived by setting the SNR value of Infinity (no noise in the signal scenario). While, in Table 6.2 the SNR value was set to $20dB$ to investigate the noise test case. In phantom measurements taken on the GOE MF II system by the manufacturer the average SNR of the 208 channels of the system attached to a phantom with wires was found to be in the range of $76.2dB$ to $84.5dB$ [22], although for experimental situations measurements much lower SNR levels have been typically observed. Therefore, a very conservative value of $20dB$ SNR was chosen for the simulation experiments. If the algorithm is able to correctly distinguish the signal at a low SNR value of $20dB$, it should have no problems working with the less noisy signal from the EIT system.

Three hyperparameter and time constant values were chosen heuristically for simulation. The columns of Table 6.1, and 6.2 represent hyperparameter values while the rows of each table represent time constant values that were used for ensemble averaging. Each cell contains the naive EIT reconstruction results on the left and the ensemble averaging results on the right. For each technique, the equivalent 4 instances of time are shown.

Table 6.1: Simulation Results For No Noise Scenario. In each cell the left column of images represents results from Naive Reconstruction and Right Column of Images represents results from Ensemble Averaging Reconstruction. Columns of Table look at simulation with 3 different regularisation hyper parameters (λ) and rows show 3 different time constants (τ). The time constant is not part of naive reconstruction, so results remain the same.

Table 6.2: Simulation Results For 20dB of Noise Scenario. In each cell the left column of images represents results from Naive Reconstruction and Right Column of Images represents results from Ensemble Averaging Reconstruction. Columns of Table look at simulation with 3 different regularisation hyper parameters (λ) and rows show 3 different time constants (τ). The time constant is not part of naive reconstruction, so results remain the same.

6.2.3   Simulation Discussion

The effects of time constant (τ) and hyperparameter (λ) can be analysed by studying the no noise scenario found in table 6.1 first. The naive reconstruction on the left column of each cell assumes that all the data points were taken at the same point in time and therefore the reconstruction of the individual frames are blurred. The ensemble averaging technique derived in this thesis incorporates a time constant τ in the expression $(e^{\frac{t_1 - t_2}{\tau}})$ which deals with this issue. When the time constant is large ($\tau = 2$ scenario) the image is blurred (leaves a trail) as the naive reconstruction. When the time constant is too small ($\tau = 0.1$ scenario) the data is thrown away prematurely and the reconstruction becomes unstable (as τ approaches zero the quotient approaches infinity) and the resulting reconstruction is inaccurate.

The hyperperameter value of the ensemble averaging technique controls the noise penalty. As the hyperparameter value is increased (from $\lambda = 0.01$ to $\lambda = 0.5$) the target in the reconstruction is blurred outwards and becomes larger in size. When the hyperparameter is decreased in size the reconstructed object is squeezed and becomes smaller in size.

Now an added noise scenario needs to be examined in Table 6.2 to view how the ensemble averaging technique handles noise. The ensemble averaging technique significantly outperforms the naive reconstruction for $\lambda = 0.5$, $\tau = 0.8$ and $\tau = 2$. The detection of target and rejection of noise is noticeable.

6.3   Human Experiments

Following the simulation study of the ensemble averaging technique three test subjects were chosen to undergo the full proposed EIT procedure in our laboratory in order to analyse the results in human studies. Two male subjects and one female subject with an age range between 26 and 36 years were chosen. Each person consented

to our EIT procedure in accordance with our ethics guidelines.

6.3.1 Human Experiments Protocol (Setup)

The EIT and ECG hardware setup in chapter 3 section 3 was implemented to obtain the simultaneous ECG and EIT data. Steps 1 to 4 described in Chapter 5 sections 5 and 5 were used offline to align the ECG to EIT and to detect QRS peaks. Then a QRS window was specified and data within this defined window around each QRS peaks were included in ensemble averaging, while the rest of the data was discarded.

6.3.2 Human Experiments Results

Based on simulation results hyperparameter value (λ=1) and time constant (τ=0.8) were chosen for experiments on test subject 1 in ensemble averaging. Figure 6.2 shows results from subject 1. While figure 6.4 and 6.6 show results from subject 2 and 3 respectively.

6.3.3 Human Experiments Discussion

Figure 6.2, (6.4, and 6.6) show ensemble averaged reconstruction from three subjects. A 1000 millisecond QRS window was chosen (500 millisecond around the R peak). Figure 6.3, 6.5, and 6.7 represent the naive reconstructions for each subject. The naive reconstruction uses a window width of -4 to 4 frames, which corresponds to a $-0.3s$ to $0.3s$ time interval around the R peak. The EIT raw data that falls within this window at each R peak is retained while the rest of the EIT signal is discarded. Then all the cardiac intervals are averaged. The goal of this analysis is to determine qualitatively if the proposed temporal ensemble averaging algorithm performs well in isolating and imaging EIT cardiac blood flow and to determine how the proposed ensemble averaging technique fares against the naive reconstruction. The data was studied to determine if the phenomena imaged is correct.
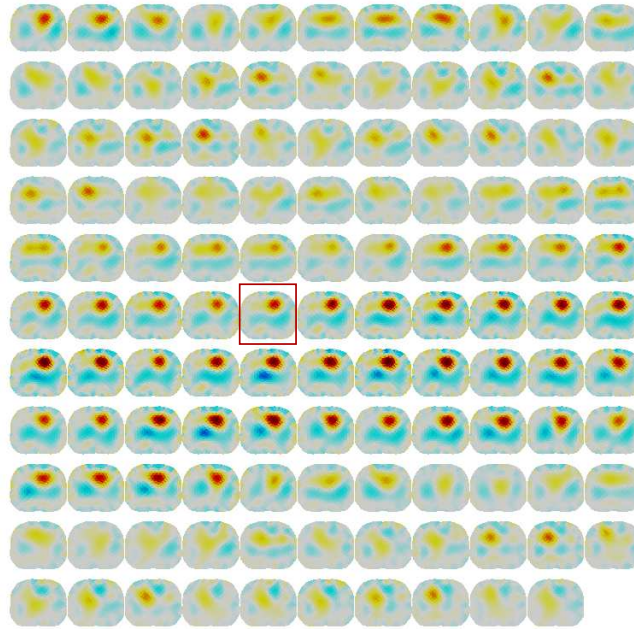
Figure 6.2: Subject 1: EIT image of ensemble averaged result of duration negative 500 millisecond to 500 millisecond around the R peak. Each image represents ten millisecond time interval. The earliest time is located top left corner, time progresses from left to right and top to bottom. The red box around the image represents the image located at the R peak.
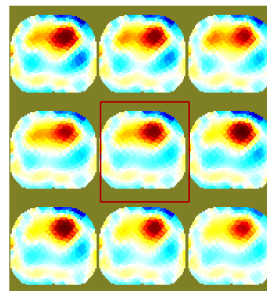
Figure 6.3: Subject 1: EIT naive reconstruction result. Averaged result for duration negative 300 millisecond to 300 millisecond around the R peak. Each image represents 77 millisecond time interval. The earliest time is located top left corner, time progresses from left to right and top to bottom. The red box around the image represents the image located at the R peak.
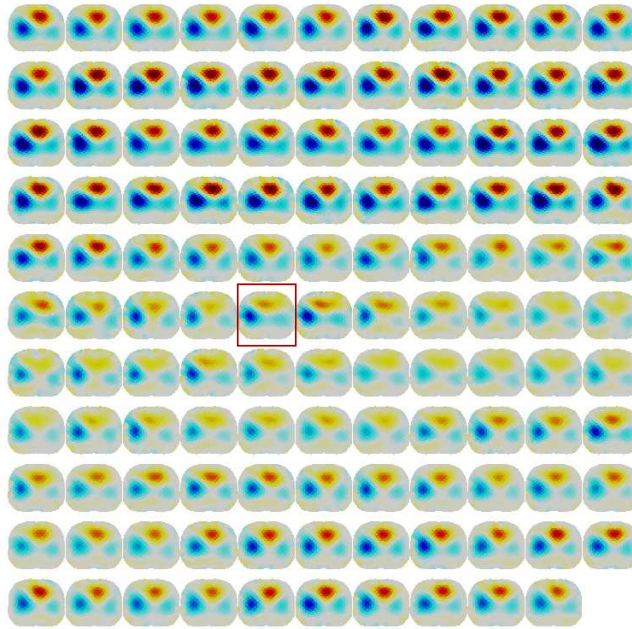
Figure 6.4: Subject 2: EIT image of ensemble averaged result of duration negative 500 millisecond to 500 millisecond around the R peak. Each image represents ten millisecond time interval. The earliest time is located top left corner, time progresses from left to right and top to bottom. The red box around the image represents the image located at the R peak.
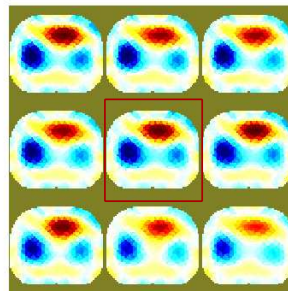
Figure 6.5: Subject 2: EIT naive reconstruction result. Averaged result for duration negative 300 millisecond to 300 millisecond around the R peak. Each image represents 77 millisecond time interval. The earliest time is located top left corner, time progresses from left to right and top to bottom. The red box around the image represents the image located at the R peak.
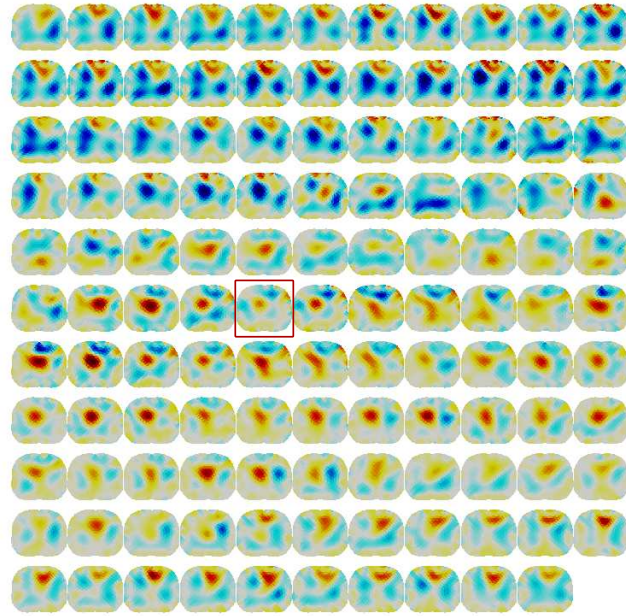
Figure 6.6: Subject 3: EIT image of ensemble averaged result of duration negative 500 millisecond to 500 millisecond around the R peak. Each image represents ten millisecond time interval. The earliest time is located top left corner, time progresses from left to right and top to bottom. The red box around the image represents the image located at the R peak.

Figure 6.7: Subject 3: EIT naive reconstruction result. Averaged result for duration negative 300 millisecond to 300 millisecond around the R peak. Each image represents 77 millisecond time interval. The earliest time is located top left corner, time progresses from left to right and top to bottom. The red box around the image represents the image located at the R peak.

In order to qualitatively analyse the results we describe the physical changes that occur during one heart cycle. Figure 6.8 and 6.9 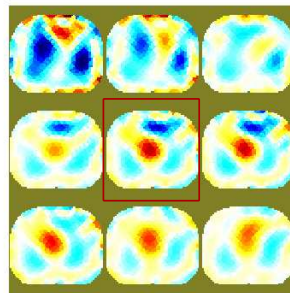depict the heart anatomy. It consists of four chambers. The upper chambers (left and right atria) and the lower chambers (left and right ventricles). The heart valves are pathways for the blood flow [36] [18]. Figure 6.10 represents the resulting electrical signal (PQRST wave) of one heart cycle. The heart beat begins at the S-A node an electrical signal is formed which travels through the atria causing an atrial contraction and blood is pushed into the ventricles. This rapid depolarisation is represented by the P wave (< 0.11 seconds in duration). Once the electrical signal reaches the A-V node time is given for the ventricles to fill. Then the electrical signal travels through the bundle of HIS and the outer Punkinje network. This causes the ventricles to contract and blood to flow to the lungs. The QRS complex represents this rapid ventricular depolarisation. The PR interval is measured from the beginning of the P wave to just before the dip at the Q signal. This interval is approximately 0.12 to 0.2 seconds in duration. While the duration of the QRS complex is only 0.05 to 0.11 seconds in duration. The T wave represents the repolarisation (recovery) of the ventricles. The ST segment and T wave time durations are not of diagnostic value and therefore are usually not measured. Only the shape of the ST segment has diagnostic value.

In Figure 6.2 the atrial contraction of the heart (P-wave) is not clearly visible. The ventricle filling and contraction pushing blood into the lungs is clearly visible in the figure. As can be seen there is a gradual change in conductivity (blood flow) in the heart region of the EIT images followed by changes in the lung region. This change in conductivity in the lungs is attributed to pulsetile blood flow through the lungs.

For Figure 6.4 and 6.6 the heart region cannot be easily identified and lung components were not entirely eliminated. There are many factors that could contribute to this. One possible explanation is that each person's heart beat has some degree of
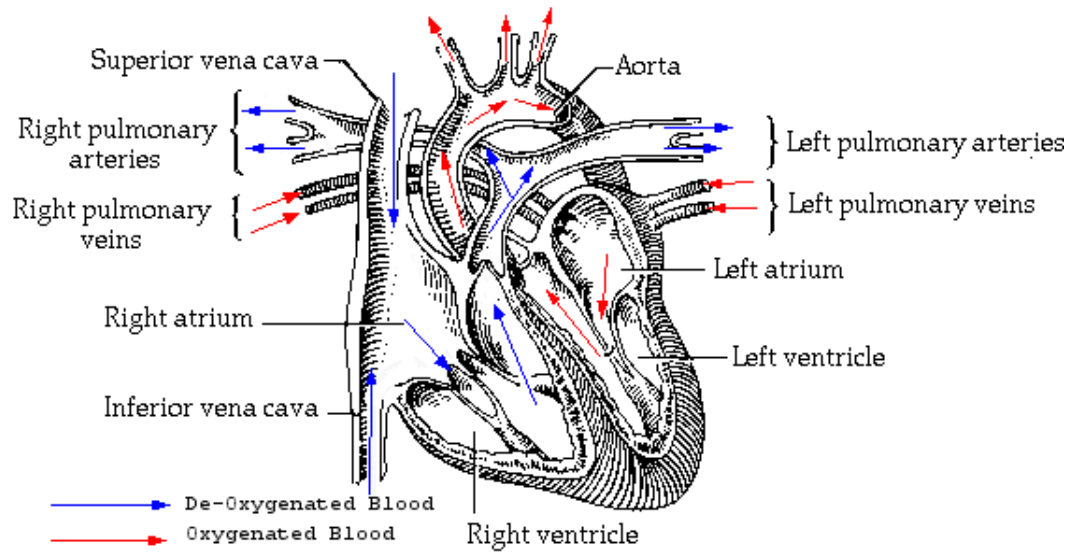
Figure 6.8: Diagram of the anatomy of the heart (reproduced from [36])
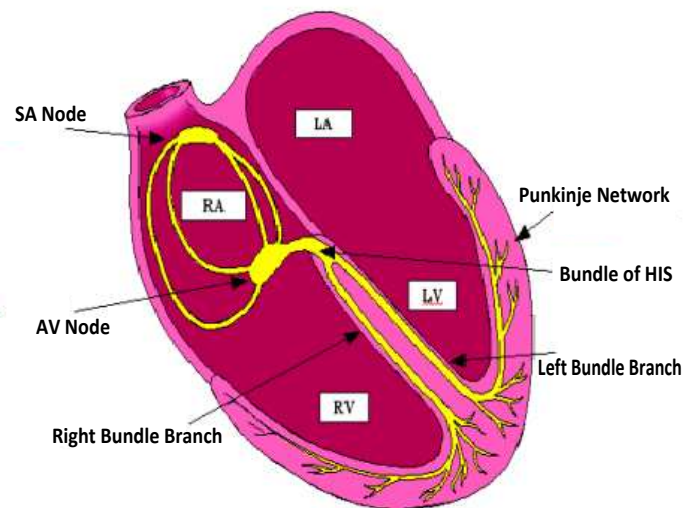
Figure 6.9: Diagram depicting the four chambers of the heart. RA represents right atrium, RV represents right ventricle, LA represents left atrium, and LV represent left ventricle (reproduced from [36]).
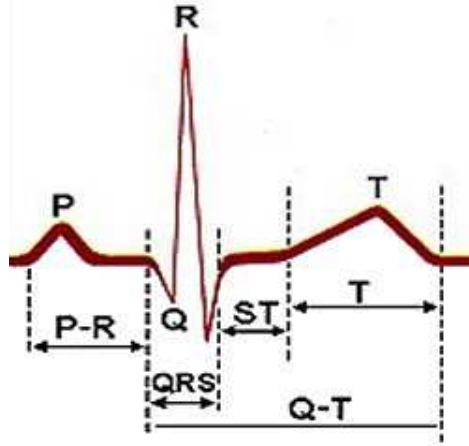
Figure 6.10: The PQRST Heart Signal with all segments (P-R, QRS, S-T, T, Q-T) annotated (reproduced from [18]).

variation or irregularity. The algorithm forces alignment of each QRS at the centre R peak but the previous and subsequent beats are not aligned due to the cardiac signal variation. Therefore, in a human cardiac cycle (with frequencies > 60 beats per minute) there will be a slight overlap from the previous and future heart beat on each end of the PQRST cycle. This will cause blurring on the images found at the beginning and cessation of each cardiac cycle. The images closest in time to the R peak should not experience any blurring. Also, the subject imaged in figure 6.4 had body hair in the measurement region while the subject imaged in figure 6.2 did not. Electrode contact impedance could have contributed to the error. The ECG readings for the subject imaged in figure 6.6 were difficult to obtain, since the PQRST wave was inverted in several measurement trials.

Examining the ensemble averaging results and the naive reconstructions for each subject it can be seen that overall both techniques yield similar images. The ensemble averaging technique proposed in this thesis has a better temporal resolution and therefore has the ability to focus on chosen windowed regions in time. Temporal resolution is defined at the smallest increment of time over which a change in an image dynamic process can be observed [21]. The time between each acquired frame

represents the temporal resolution of the naive reconstruction. The naive reconstruction can only reconstruct one image per frame. The GOE MF II EIT system has an acquisition rate of 13 frames per second. Therefore, the temporal resolution of the naive reconstruction is $76.9ms$. The temporal resolution for the algorithm derived in this thesis is controlled by parameter τ because the algorithm is able to predict images at times where EIT data was not acquired based on nearby data. The images of the ensemble solver for the experiments where calculated with a temporal resolution of $50ms$. A good temporal resolution is very important when imaging a fast moving phenomena such as cardiac activity. Being able to focus on specific parts of the cardiac cycle in time can assist in monitoring anomalies that could lead to a diagnosis.

6.4   Experiments Summary

In software simulation trials it was shown that the proposed temporal ensemble averaging algorithm performs better than naive reconstruction in high noise scenarios (if time constant and hyperparameter are set properly). In the human testing the algorithm did not perform well on all subjects. The algorithm does show potential in subject 1 and 2. The naive reconstruction performs to the same degree in human trials but the novel algorithm has a greater temporal resolution. A larger pool of patients is required to conclusively demonstrate the performance of the ensemble averaging technique.

Chapter 7

Conclusion and Future Work

7.1 Summary of Contributions

Heart disease affects a large population in Canada [13]. Most Canadians suffering from heart disease are diagnosed with Coronary Artery Disease (CAD). Coronary Angiogram and cardiac CT are the gold standard methods of diagnosing CAD. Both of these methods are invasive, expensive and cannot be used for monitoring purposes. Therefore, scientists and physicians alike are searching for an inexpensive, non invasive, portable tool of diagnosis and monitoring. EIT is an experimental imaging modality that uses electrodes placed on the body to infer the conductivity distribution of applied current in the underlying tissue [6]. EIT is inexpensive, safe, non-invasive and boasts a small form factor making it ideal for portable monitoring purposes. EIT also has a high temporal acquisition rate which is required to monitor cardiac activity. EIT hardware has improved and the depth of knowledge and techniques used for cardiac EIT have come a long way [29]. Recently there has been exciting new developments in estimation of cardiac output using EIT.

The purpose of this thesis was to develop a collection of techniques for the study of cardiac EIT measurements at UOHI. To accomplish this goal the existing Cardiac

CT protocol was examined and an EIT protocol was developed to work with it. Afterwards a hardware toolset was designed to aid in collection of EIT data. An ECG amplifier was built for simultaneous ECG and EIT data collection. A hardware sync pulse was implemented for ECG and EIT synchronisation. Then a software toolset was designed to prepare the EIT data for the final step. This software toolset included filtering of the raw ECG date for noise and R peak detection. A portion of this software toolset was used to filter the EIT data for known hardware anomalies and alignment to ECG data. A novel temporal ensemble averaging technique was derive to extract the cardiac portion of the EIT data. Finally the ensemble averaging technique was tested in simulation trials and human trials to examine its validity.

7.2 Conclusion

A toolset for EIT cardiac research was created in this thesis. This toolset was designed to commence research at UOHI. The results from simulation of the novel temporal ensemble averaging technique have shown that the technique is more resilient to noise than naive reconstruction. The EIT protocol, hardware setup, software setup, and novel temporal ensemble averaging algorithm were tested in a preliminary human trial. The human trials were inconclusive. The ensemble averaging reconstruction worked extremely well for one subject. The second subject showed a bit of improvement. While the third subject cardiac EIT reconstruction was poor. There are many possible factors for this, such as: the subject did not hold their breath properly, the patient has arhythmia, the EIT and ECG signals are not aligned properly, EIT hardware artifact that is not adequately filtered, and electrode contact problems. More human trials need to be performed in future work in order to determine the actual performance of this algorithm. The EIT protocol, ECG amplifier, hardware sync pulse, and software data preparation techniques met requirements.

7.3 Future Work

Now that this thesis has designed a collection of techniques to acquire and analyse EIT cardiac data these tools are ready for implementation in UOHI. The following recommendations are made for future work on this research.

The first recommendation is to devise a method of comparison for EIT and CT images as it regards to blood flow through the heart. In this thesis the EIT images were studied qualitatively to determine if the toolset was able to isolate and image any cardiac activity. The methods in the toolset were designed to incorporate the gold standard CT scans in a comparison analysis. For instance the EIT measurements have been synced to an ECG signal which can be used for CT to EIT image registration. Correlation between the CT and EIT images need to be studied in order to quantitatively determine if EIT is a useful tool for cardiac monitoring.

The second recommendation is to test the proposed toolset on patients at UOHI. This toolset was only studied with a limited volunteer set to analyse if the techniques produced promising results. Now they are ready for a test run in the environment the toolset was designed for. The toolset was only tested on healthy volunteers and it would be interesting to determine if there are visible changes with patients that have pre-existing cardiac conditions.

Next there is a need to tweak the EIT protocol and temporal ensemble averaging technique to achieve optimal cardiac EIT images. Using the before stated recommendations after formulating the CT and EIT comparison and performing tests on UOHI patients the researcher might find ways to tweak the existing EIT protocol to improve efficiency or to allow for more accurate and consistent measurements. For instance if four electrodes are not enough to mark the locations of the EIT electrode plane on the CT scans more electrodes might need to be added. If too many EIT data acquisition trials exhibit bad electrode contact screening methods might have to be imposed if solutions cannot be devised. The EIT image resolution can be improved by tweak-

ing the hyperperameter parameter and time constant values. Thus far these have been tweaked manually but CT comparisons might give way to automatic methods of determining the correct value for each patient.

Another recommendation is to include other known EIT methods to improve cardiac EIT imaging. As for example the addition of hypertonic saline as an EIT image contrast agent [29]. Hypertonic saline would constitute a minimal risk but the EIT procedure would become more invasive [29]. In the cardiac CT study at UOHI the patients under go CT imaging procedure were an IV is inserted. Therefore, when piggy backing on this study the degree of invasiveness will not increase. The physician has requested experimental support in order to consider the administration of hypertonic saline during EIT imaging. Other than the addition of hypertonic saline as a contrast agent there are several studies that have made great strides in measuring cardiac output. Only a subset (ensemble averaging, breath hold and ECG gating [29]) of those techniques were implemented in this thesis toolset. The additions of other methods (optimised separation in the temporal and spatial domains (OSTSD), impedance time curves, parametric EIT [29]) from these experiments might benefit this study. OSTSD deals with separating the EIT respiratory signal from the cardiac signal using frequency and the spatial heart region and can be is often used instead of ECG gating [29]. In order to do this one can study the fourier spectrum of the heart region [29]. Impedance time curves have been used to measure stroke volume in EIT images [29]. This method deals with averaging several hundred heart cycles to extract width and height of the averaged impedance time curves [29]. Once these parameters are found the following equation 7.1 can be used to measure the stroke volume [29]. Where A_{ROI} is the pixel area of the region of interest (heart region), and C_1 and C_2 are stroke volume calibration constants [29]. Instead of impedance time curve method parametric EIT method can be used to measure stroke volume [29]. From CT images physical measurements of the heart region can be made and one can

represent the heart region as 2D ellipsoid with corresponding parameters [29]. This ellipsoid can be used to estimate the left ventricular volume, V_{LV} using the ellipsoid single plane area length model shown in equation 7.2 [29]. Where r_{minor} is the short axis and r_{major} is the long axis on the ellipsoid [29]. Achieving accurate measurements of stroke volume can guide in diagnosing CAD at UOHI.

$$Stroke\ Volume = C_1 \cdot W \cdot \sqrt{H \cdot A_{ROI}} + C_2 \qquad (7.1)$$

$$Stroke\ Volume = \frac{8(\pi \cdot r_{minor} \cdot r_{major})^2}{3\pi \cdot r_{major}} \qquad (7.2)$$

Perfecting the protocol for the GOE MF II EIT system one can later implement the EIT protocol with different EIT systems as well in order to observe any imaging improvements. Each EIT system has its own characteristics. One system could theoretically possess more desirable cardiac images. For instance there are several EIT systems in the Carleton laboratory. They each have different acquisition rates, different ways of handling electrodes, different methods of acquiring the data (stimulation pattern, etc), and different methods of transmitting the data. The new EIT system designed in Montreal has shown better resolution in preliminary tank study in our lab. Also, the system will have integrated bluetooth in the next version. This can be used as a hardware sync to ECG gating instead of the RC circuit. It would be interesting to see what each system has to offer as it pertains to cardiac EIT imaging.

Once the toolset in this thesis has properly evolved and cardiac EIT images are optimal (or acceptable) the next step is to increase the number of patient EIT and CT images. Diagnostic tools used in a medical setting need to be consistent and the exclusion criteria needs to be well known. Therefore, a large data set of subjects needs to be studied. Also, it is a wonderful opportunity to collect data from patients with pre-existing cardiac conditions, since, most studies have focused on healthy volunteers.

Having a large dataset of CT and EIT images would be invaluable in further study of EIT and it's characteristics. CT images offer excellent structural data which can be used to EIT mesh design and there are other physiological parameters that can be studied from CT images such as lung perfusion. Developments in EIT imaging could potentially result in improved bedside cardiac monitoring, which can benefit cardiac patients in timely diagnosis and treatment.

Appendix A

A.1 UOHI Ethics Protocol

<div align="center">**Patient Information Sheet and Consent Form**</div>

<div align="center">**Assessment of left ventricular ejection fraction and regional wall motion with Cardiac Computed Tomography**</div>

<div align="center">**UOHI Protocol # 2006917-01H**</div>

Co-Principal Investigators

Dr. Benjamin Chow	613-761-4044

Co-Investigators

Dr. Terrence Ruddy	613-761-4085
Dr. Luc Beauchesne	613-761-4422
Dr. Andy Adler	613-520-2600 ext 8785

Research Co-ordinators

Mary Dalipaj	613-761-5474
Yeung Yam	613-761-4044
Sandina Jamieson	613-761-4044

Please read this Patient Information Sheet and Consent Form carefully and ask as many questions as you like before deciding whether to participate.

Introduction:

You have been invited to participate in a research project entitled: *Assessment of left ventricular ejection fraction and regional wall motion with Cardiac Computed Tomography.* The purpose of this project is to examine the accuracy of cardiac CT (x-ray machine that gives very detailed images of the heart and its blood vessels) in determining left ventricular ejection fraction (LVEF) and ventricular regional wall motion. Both of these measurements help us determine how well your heart is functioning. Therefore, the results from the CT scan will be compared with radionuclide ventriculography (nuclear imaging using radioactive $^{99m}TcO_4$- (pertechnetate) to label your blood cells to assess the amount of blood in your heart before and after it empties). 2D echocardiography (an ultrasound image of your heart) to determine how well CT can assess heart motion, or Electrical Impendence Tomography (EIT) which measures electrical signals from your heart.

Your Cardiologist has identified you as a candidate for this study. You are currently awaiting or recently had cardiac CT. If agreeable, you will undergo an additional radionuclide ventriculography scan and 2D echocardiography of the heart and/EIT. The information gathered will be compared with your recent cardiac CT. We will enroll fifty patients in this pilot study.

Background:

Currently, at the University of Ottawa Heart Institute, the "gold standard" for the assessment of left ventricular ejection fraction is radionuclide ventriculography, while the current "gold standard" for assessment of regional wall motion is 2D echocardiography. Cardiac CT is a new technology which may enable the evaluation of your coronary anatomy without exposing you to the risks of invasive cardiac catheterization. If cardiac CT can be used to assess LVEF and regional wall motion, this may reduce the number of tests that patients like yourself would have to undergo.

We will enroll patients who are awaiting or who have previously undergone cardiac CT. Consenting patients will also undergo radionuclide ventriculography and 2D echocardiography. These additional tests will require approximately 4-6 hours of your time and will be scheduled on two different days.

Procedure:

You will be asked to avoid caffeine for 12 hours prior to your testing and to fast (except for medications) for 4 hours before the CT and radionuclide ventriculography scan.

Cardiac CT

If you agree to participate in the study, you will have a CT scan at the University of Ottawa Heart Institute. On arrival, you will meet with a nurse who will ensure that you can safely proceed with the study. An intravenous will be placed in one arm. If you are at risk for kidney dysfunction, two teaspoons (10 mL) of blood will be drawn to assess you kidney function. You will then be positioned on the CT scan bed and your heart rhythm and blood pressure will be monitored. If required, your heart rate will be slowed with intravenous metoprolol (B-blocker). This will be administered under the supervision of a Cardiologist from the University of Ottawa Heart Institute. X-ray dye will be infused intravenously. You will be asked to hold your breath for 10 seconds while the CT scan images are acquired. Once the images have been acquired, your CT scan is complete.

Electrical Impedance Tomography

EIT measured will be taken simultaneously with the Cardiac CT measurements. Sixteen ECG-type electrodes will be placed around your chest, and connected with wires to the scanner. During the CT scan, a very low power electrical signal will be transmitted into your body and electrical measurements will be made at the electrodes.

Radionuclide Ventriculography Scan

All patients will undergo a radionuclide scan. An intravenous line will be placed in your arm so that a radioactive isotope can be injected into your vein. The radioactive isotope will then attach to red blood cells and pass through the heart in the circulation. The radioactive isotope can be traced through the heart using special cameras placed over your chest.

2D-Echocardiography

All patients will undergo echocardiography as well. This test uses sound waves to create a moving picture of the heart. The picture is much more detailed than an x-ray

image and allows doctors to see the heart beating and visualize many of the structures of the heart. An instrument that transmits high-frequency sound waves called a transducer is placed on your ribs near the breast bone and directed toward the heart. The transducer picks up the sound waves and transmits them as electrical impulses. The echocardiography machine then converts these impulses into moving pictures of the heart.

Risks and Discomforts of Participation:

We do not anticipate any significant harm from this study. You may experience some discomfort with the insertion of the intravenous catheter (a small tube placed in a vein used to give fluids and medications). There is a small risk of bruising and infection with an intravenous catheter.

Cardiac CT

We do not anticipate any adverse effects from the x-ray dye during a CT scan. The risks of x-ray dye are small and include hives (skin rash and swelling) (2%) and allergic reaction (0.1%) Intravenous metoprolol is a very common medication and is routinely used at the University of Ottawa Heart Institute. It can result in low heart rates and blood pressure however these parameters will be closely observed by a Staff Cardiologist from the University of Ottawa Heart Institute.

Electrical Impedance Tomography

We do not anticipate any adverse effects from EIT measurements. The electrical signals used cannot be felt and the technology is safe.

Radionuclide Ventriculography (RNV)

Radionuclide ventriculography is an imaging techniques that involves a small dose of a radioactive substance that will be given intravenously (through a vein). You may notice a metallic taste for a few seconds after injection has occurred. All patients undergo standard safety measurements, blood pressure, continuous heart rate monitoring and evaluation of possible side effects throughout the imaging procedure. The total radiation dose (RNV and CT) that you will receive from this study is equivalent to the amount a person would receive naturally while living in Ontario for 8 – 9.5 years. The radiation dose is considered safe and well within the accepted guidelines. There are no expected consequences associated with this exposure.

2D-Echocardiography

This test does not involve any exposure to radioactivity, and is not associated with any known risks. During this procedure, the probe pressed against your chest to acquire ultrasound images may cause slight chest tenderness.

Pregnancy Risk:

It is known that in early pregnancy radiation exposure may harm the fetus and therefore CT and RNV scans are not performed in women who may be pregnant. A urine

pregnancy test will be performed, on all females of child-bearing potential to rule out pregnancy. Women must agree to try <u>not</u> becoming pregnant during their two week participation in this study. In the event of pregnancy, or suspected pregnancy at the time of the scan, you must tell the study coordinator immediately and you must agree <u>not</u> to have the scan.

Benefits of Participation:

You may not receive any direct benefit from your participation in this research. Your participation in this research may allow the researchers to better define the role of Cardiac CT at the University of Ottawa Heart Institute. This may benefit future patients because the risks of invasive cardiac catheterization may be avoided.

Confidentiality:

All the results of the study will be kept confidential. The investigators of this project will have access to the results of your tests. Your health records may also be reviewed by members of the Heart Institute Human Research Ethics Board under the supervision of the Investigator or his/her staff. Under no circumstances will records bearing your name leave the Ottawa Heart Institute. You will not be identifiable in any publications resulting from this study. Any information can be made available to your family doctor if you request it. Your test results will be kept on file in the Ottawa Hospital Radiology Department or the University of Ottawa Heart Institute. The results of the study will be securely kept at the University of Ottawa Heart Institute.

Ethics:

The radiation aspect of this protocol was reviewed by the Isotope & X-Ray Committee of the Ottawa Hospital, Civic Campus and approval is given for the protocol to be presented for approval by the Heart Institute Human Research Ethics Board. The Human Research Ethics Board (HREB) of the University of Ottawa Heart Institute has approved this protocol. The HREB considers the ethical aspects of all Heart Institute research projects involving human subjects. If you wish, you may talk to the Chair, Human Research Ethics Board at 613-798-5555, ext 19865.

Participation:

Participation in research is completely voluntary. You are free to choose to participate or not to participate in this research study. If you agree to participate in this study, you may choose to withdraw you participation at any time. This will not affect your present or future care at the Heart Institute, or at any hospital. You may also refuse to answer any specific questions.

Consent to Participate in Research

I understand that I am being asked to participate in a research study about **Comparison of cardiac CT with radionuclide ventriculography and 2D-echocardiography**. This study has been explained to me by _____.

I have read and understood this 5 page Patient Information Sheet and Consent Form. All my questions at this time have been answered to my satisfaction. If I or any of my family members have any further questions about this study, we may contact Sandina Jamieson at 613-761-4044.

I will receive a signed copy of this Patient Information Sheet and Consent Form.

I voluntarily agree to participate in this study.

Patient's Name   _____

Patient's Signature   _____

Date   _____

Signature of Person Obtaining Consent _____

(Co-)Investigator's Signature   _____

Date   _____

Appendix B

B.1 Matlab Code: Software Toolset

```
%function readcsv used to read in the .csv file containing the PicoScope
%oscilloscope data and eliminate %60Hz frequency from signal and band
%pass filter signal from 10Hz to 50Hz (portion that is cardiac data)
%this function represents Steps 1 and 2 in our software toolset
%@input: dname ,fname,fnum, proc
%@return: t,d1,d2
%dname holds the name of the directory the file is located in,
%fname is the filename, fnum contains  the %number of parts the
%file is broken into, proc contains an integer representing  the
%type of filtering that %is desired, t returns duration of csv signal
%acquisition in seconds, d1 holds the ECG data, d2 holds the
%Sync Pulse data
function [t,d1,d2]=readcsv(dname, fname, fnum, proc)
     ts=[]; d1=[]; d2=[];
     for fn = fnum;
        fnread = sprintf(fname,fn);
        ff= csvread([dname,'/',fnread],2);
        subs = 1:100:size(ff,1); % SUBSAMPLE
        d1=[d1; ff(subs,2)];
        d2=[d2; ff(subs,3)];
        ts_est = diff(ff(subs(1:2)));
        if isempty(ts);
           ts = ts_est;
        else
           if ts ~= ts_est; error('inconsistent sample rate'); end
        end
     end
     t = (0:length(d1)-1)*ts;
```

```
   fs = 1/diff(t(1:2)); %sampling freq
   switch proc
     case 0 ; return
     case 1 ; d1= elim_freq( d1, fs, 60, 2); % eliminate 60 Hz
%eliminate 60 Hz in sub-sampled signal
     case 2 ; d1= elim_freq( d1, fs, 12.6, 2);
     case 3 ;
        d1= elim_freq( d1, fs, 12.6, 2);
%band pass filter between 10 Hz and 50Hz
        d1= bpf( d1, fs, 10, 50);
     case 4 ;
        d1= bpf( d1, fs, 12.4, 12.7);
     otherwise ;
        error('huh?');
   end


%function qrs_detect detects all the R peaks in the ECG signal.
%This is step 3 in the software toolset
%@input ts,d
%@return idx
% ts is sample rate, d is the ecg signal, idx hold the R peak times
function [idx]=qrs_detect(ts,d)
   dm = d - mean(d);
   ld = length(d);
   % SET THRESHOLD at 98% point (2% of signal is R wave)
   ss = sort(dm);
   thresh = ss(round(0.98*ld));
   st = sparse(dm.*(dm>thresh));
   elimw= round(0.1/ts); % No QRS within 0.1s
   idx= [];
   while any(st)
     [jnk,idxi]= max(st);
     idxi=idxi(1); idx= [idx, idxi];
     mine = max(idxi-elimw,1);
     maxe = min(idxi+elimw,ld);
     st(mine:maxe)=0;
   end
   idx = sort(idx);
   space = ts*diff(idx);
   shortbt = find( space<0.5 );
   idx([shortbt,shortbt+1]) = [];


%function findstart_end locates the start and end time of the
%sync pulse signal.  This function represents %step 4 in the
%software toolset.
```

```
%@input t,d2,thresh
%@return tstart, tend
%t the time duration of the sync pulse signal in seconds, d2 sync
%pulse signal, threshold for start and end %detection
function [tstart,tend]=findstart_end(t,d2,thresh)
    if nargin<3; thresh= [5,5]; end
    [tstart]=findstart(t,d2, thresh(1));
    thresh(2)
    [tend]=  findstart(flipud(t(:)),flipud(d2(:)), thresh(2));

function [tstart]=findstart(t,d2, thresh)
    dt = abs(diff(t(1:2)));
    % get first 2 seconds properties of sync signal (baseline)
    sec_1 = 1:round(2/dt);
    mean_sec_1 = mean(d2(sec_1));
    std__sec_1 = std(d2(sec_1)) ;
    sig_t  = abs(d2-mean_sec_1) > thresh*std__sec_1;
    ff= find(sig_t); ff=ff(1);
    tstart = t(ff);

%function eit_data_test reads in EIT data, shifts it to sync pulse
%start time and end time, and marks the %ECG R peaks in the breath
%hold section.  This is step 5 and 6 of the software toolset.
function [img, vi, vh]=eit_data_test(fname, times)
    rm= mk_rec_alg(1);
    [vi,vh]= read_data(fname);
    img= inv_solve(rm, vh, vi);
    sigl = size(vi,2);
    t = linspace(times.ts,times.te, sigl);
    sig= sum(img.elem_data);
  axes('position',[0.05,0.05,0.9,0.2]);
    plot(t,sig);
    xlim([0,65]);
    ylim([min(sig),max(sig)]);
    title('(d)');
    set(get(gca, 'title'),'FontWeight', 'bold');
    ylabel('millivolts (mV)');
    xlabel('time (s)');
    avg= [];
    width= -4:4;
    for tqrs=times.qrs_locn
        if tqrs > times.te; break ; end
        [jnk,idx] = min( abs(t - tqrs));
        if max(idx+width) > sigl; break; end
        hh= line(tqrs*[1,1], ylim); set(hh,'Color',[0,0,0]);
```

```
        avg= cat(3, avg, img.elem_data(:, idx+width));
    end

%function read_data reads in EIT data and fixes known Viasys EIT
%artifact.  This is step 5 in the software %toolset
%@input : fname
%@return: vi,vh
%fname is the file name for the EIT data file, vi difference
%data sequence of times, vh difference data %assumed homogenous
function [vi,vh]= read_data(fname)
    [dpath,fn] = data_locn(fname);
    fname= [dpath,'/',fn];
    vi= eidors_readdata( fname );
    vi = edit_artefacts( vi , fname);
    ll = size(vi,2);
% reference is inspiratory breath hold for last half
    vh= mean( vi(:, round(ll*.65):end), 2);

%function mk_rec_alg choice of reconstructive mesh is made
%for EIT image reconstruction
function rm = mk_rec_alg( no )
    switch no
      case 0;
        rm= mk_common_gridmdl('b2c','GREITc1');
      case 1;
        rm= mk_common_model('c2t2');
        rm.fwd_model.normalize_measurements=1;
      case 2;
        rm= mk_common_model('c2t2');
        rm.fwd_model.normalize_measurements=1;
        rm.fwd_model.jacobian = @calc_move_jacobian;
        rm.RtR_prior =         @aa_e_move_image_prior;
        rm.aa_e_move_image_prior.parameters = sqrt(1e-3/1);
% Don't show move params
        rm.inv_solve.select_parameters = 1:576;
      otherwise;
       error('huh?');
    end

%function edit_artifact looks for sharp changes in a single
%channel for the EIT data
function data= edit_artefacts( data, fn )
    for i=1:256
        dc = data(i,:);
```

```
      if norm(dc) < 1e-4; continue; end
      qq= quartiles( dc );
      ff= find( abs(diff(dc))  > 3*(qq(3)-qq(1)) );
      ff= find( abs(dc - qq(2) )  > 4*(qq(3)-qq(1)) );
      if ff
        fprintf('FILE (%s) CHANNEL (%d) Artefact\n', fn, i);
        dc(ff) = qq(2);
        data(i,:) = dc;
      end
    end

function qq= quartiles( dd )
   ds= sort( dd );
   qq= interp1( linspace(0,1,length(dd)), ds, [.25,.5,.75] );



% ENSEMBLE_SOLVE inverse solver using ensemble average.  This
% function is the  novel temporal %ensemble average algorithm
% derived in Step 7 in software toolset.
% img= aa_inv_solve( inv_model, data1, data2)
% img        => output image (or vector of images)
% inv_model  => inverse model struct
% vh         => difference data assume homogemeous
% vi         => difference data at sequence of times
%
% inv_model.ensemble_solve.solve_times = [ .... ]
% inv_model.ensemble_solve.t_const     =
function img= ensemble_solve( inv_model, vh, vi)
[J,hp,L] = calc_inv_term( inv_model);
[Nn,Nt] = size(vi.meas);
if 0
  dv = calc_difference_data( vh, vi, inv_model.fwd_model);
else
  dv = vi.meas - vh.meas*ones(1,Nt);
  if inv_model.fwd_model.normalize_measurements;
    dv = dv ./ (vh.meas*ones(1,Nt));
  end
end
tm = vi.time(:); tm = tm*ones(1,length(tm));
expp= abs(tm-tm')/inv_model.ensemble_solve.t_const;
expp(expp>10) = inf; % Set to inf so exp is 0
gamma = sparse( exp(-expp) );
Sn    = hp^2*speye(prod([Nn,Nt]));
JSxJt = kron(ones(Nt),J*L*J');
full_JSxJt_Sn = gamma.*JSxJt + Sn;
```

```
tm =     vi.time(:)';
times = inv_model.ensemble_solve.solve_times(:);
Ntm   = length(times);
tm = ones(size(times))*tm - times*ones(size(tm));
expp= abs(tm)/inv_model.ensemble_solve.t_const;
expp(expp>10) = inf; % Set to inf so exp is 0
gamma = kron( sparse( exp(-expp) ), ones(size(J,2),1) );
SxJt = kron(ones(Ntm,Nt),L*J');
full_SxJt = gamma.*SxJt;
sol = full_SxJt * ( full_JSxJt_Sn \ dv(:) );
sol = reshape(sol, [], Ntm);
% create a data structure to return
img = eidors_obj('image','solved by ensemble_solve');
img.elem_data = sol;
img.fwd_model= inv_model.fwd_model;

function [J,hp,L] = calc_inv_term( inv_model);
    fwd_model= inv_model.fwd_model;
    pp= aa_fwd_parameters( fwd_model );

    img_bkgnd= calc_jacobian_bkgnd( inv_model );
    J = calc_jacobian( fwd_model, img_bkgnd);

    L = inv(calc_RtR_prior( inv_model )); % Lambda
    hp  = calc_hyperparameter( inv_model );
```

B.2   Matlab Code: Simulation Experiment

```
% [VH,VI]= SIM_MOVE( FRAME_REV, SNR )
% Simulate movement of a small object
%  vh, vi = homog and inhomog movement vectors
%  frame_rev = frames / revolution
%  SNR = signal to noise ratio (default 0 noise)
%  frames = frames to siulates (defaults = 100)
function [vh,vi]= sim_move( frame_rev, SNR, frames )
if nargin < 3; frames = 100; end
if nargin < 2; SNR    = Inf; end
mdl = mk_model(1);
xyr = sim_path(frame_rev, frames);
[vh,vi,signal] = sim_and_remove( mdl, xyr, frames);
randn('seed',5);
vi.meas = vi.meas + signal/SNR*randn( size(vi.meas) );
```

```
%Setting the measurements per frame of the simulation to 208
function MPF= meas_per_frame; MPF = 208;
%sim_path  and sim_and_remove functions simulates the target movement
function xyr = sim_path(frame_rev, frames)
  prad = 0.6; orad= 0.1;
  angl = linspace(0,2*pi*frames/frame_rev, frames*meas_per_frame+1);
  angl(end)=[];
  xyr  = [prad*sin(angl); ...
          prad*cos(angl); ...
          orad*ones(1,length(angl))];
function [vh,vi,signal] = sim_and_remove( fmdl, xyr,frames);
  img = eidors_obj('image','sim');
  img.fwd_model = fmdl;
  img.elem_data = ones(size(fmdl.elems,1),1);
  [vh,vifull]= simulate_movement( img, xyr);
  signal = sqrt(std(vh - vifull(:,1)));
   vh = eidors_obj('data','homog','time',-1,'meas',vh);
% Collect a measurement each frame
  tfac = size(xyr,2)/frames; % # frames units
  vi = eidors_obj('data','homog');
  vi.time = zeros(meas_per_frame, frames);
  vi.meas = zeros(meas_per_frame, frames);
  idx = 0;
  for f = 1:frames;
     for i = 1:meas_per_frame;
        vi.time(i,f) = idx/tfac;
        idx = idx + 1;
        vi.meas(i,f) = vifull(i,idx);
     end
  end
%mk_model function allows for selection of type of mesh model
%and electrode layout and stimulation %pattern
function fmdl = mk_model( type )
  switch type
    case 1;
      imdl = mk_common_model('f2C2',16);
      fmdl = imdl.fwd_model;
    case 2;
      fmdl= ng_mk_cyl_models([0,1,0.1],[16],[0.2,0,0.02]);
    otherwise; error('mk_model; huh?');
  end
```

Bibliography

[1] Zainul Abendin and Enrique Carbajal. Frequency analysis of the pqrst complex of the normal electrocardiogram. *Journal of Clinical Engineering*, 8, 1983.

[2] Andy Adler. Advances in image reconstruction in electrical impedance tomography. OCIBME Seminar, Carleton University, Ottawa, Canada, 25 Oct 2005.

[3] Andy Adler. Biom5100 lecture: Amplifier design. attended November 10, 2007.

[4] Andy Adler. Biom5100 lecture: Ecg electrocardiogram. attended September 24, 2007.

[5] Andy Adler. Electrical impedance tomography: advances in image reconstruction. EIT Workshop, Haarlem, Netherlands, 3 Nov 2006.

[6] Andy Adler. Electrical impedance tomography: Image algorithms and applicationsn. BIOM 5200: Medical Imaging.

[7] Andy Adler, John H Arnold, Richard Bayford, Andrea Borsic, Brian Brown, Paul Dixon, Theo J C Faes, Inez Frerichs, Herve Gagnon, Yvo Garber, Bartlomiej Grychtol, Gunter Hahn, William R B Lionheart, Anjum Malik, Robert P Patterson, Janet Stocks, Andrew Tizzard, Norbert Weiler, and Gerhard K Wolf. Greit: a unified approach to 2d linear eit reconstruction of lung images. *Institute of Physics and Engineering in Medicine*, 30:S35–S55, 2009.

[8] Joerg Barkhausen, Raimund Erbel, Karl-Friedrich Kreitner, and Manfred Thelen. *Cardiac Imaging: A Multimodality Approach*. Thieme, New York, 2009.

[9] Andrew Binley, William Daily, Douglas LaBrecque, and Abelardo Ramirez. *Chapter 17, Electrical Resistance TomographyTheory and Practice*. SEG, 2005.

[10] Mathew J. Budoff and Jerold S. Shinbane. *CardiacCT Imaging*. Springer-Verlag London Limited, Singapore, 2006.

[11] Shawn Carlson. Home is where the ecg is. *Scientific American*, June 2000, 2000.

[12] M Cheney, D Isaacson, JC Newell, S Simske, and JC Globle. Noser: an algorithm for solving the inverse conductivity problem. *Int J Imaging Syst Technol*, 2:66–75, 1990.

[13] Benjamin JW Chow, Udo Hoffmann, and Koen Nieman. Computed tomographic coronary angiography: An alternative to invasive coronary angiography. *Can J Cardiol*, 21(11):933–940, 2005.

[14] John Jr. Clark, Michael Neuman, Walter Olson, Robert Peura, Frank Jr. Primiano, Melvin Siedband, John Webster, and Wheeler Lawrence. *Medical Instrumentation (Application and Design)*. John Wiley and Sons, Inc., 111 River Street, Hoboken, NJ, 3rd edition, 1998.

[15] United States Nuclear Regulatory Comission. Doses in our daily lives. `http://www.nrc.gov/about-nrc/radiation/around-us/doses-daily-lives.html`.

[16] Tao Dai. *Image Reconstruction in EIT Using Advanced Regularization Frameworks*. Department of Systems and Computer Engineering, Carleton University, Ottawa, Ontario, 2008.

[17] Analog Devices. Precision instrumentation amplifier ad624, 1999. Rev. C.

[18] Westside Enterprises. The electrocardiogram. `http://www.tveatch.org/ekgs/pqrst.html`.

[19] David S. Holder etal. *Electrical Impedance Tomography, Methods, History and Applications*. IOP Publishing Ltd, Bristol and Philadelphia, 2005.

[20] Mayo Foundation for Medical Education and Research. Coronary artery disease: Treatments and drugs. `http://www.mayoclinic.com/health/coronary-artery-disease/DS00064/DSECTION=treatments-and-drugs`.

[21] Slavin GS and Bluemke DA. Spatial and temporal resolution in cardiovascular mr imaging: review and recommendations. *Radiology*, 232:330–338, 2005.

[22] G. Hahn, Just A., and G. Hellige. Determination of the dynamic measurement error of eit systems. *IFMBE Proceedings*, 17:320–323, 2007.

[23] Bruce H. Hasegawa. *The Physicas of Medical X-Ray Imaging*. Medical Physics Pub., 1991.

[24] Heart and Stroke Foundation. Statistics. `http://www.heartandstroke.on.ca/site/c.pvI3IeNWJwE/b.3581729/k.359A/Statistics.htm#heartdisease`.

[25] Heart and Stroke Foundation. What is heart disease? `http://www.heartandstroke.com/site/c.ikIQLcMWJtE/b.3682421/k.48B2/Heart_disease__What_is_heart_disease.htm`.

[26] R.P. Henderson and J.G. Webster. An impedance camera for spatially specific measurements of the thorax. *IEEE Trans. Biomed. Eng.*, 25:250–254, 1978.

[27] Colin Howson and Peter Urbach. *Scientific Reasoning: The Bayesian Approach*. Open Court Publishing Company, 1993.

[28] BU Kohler, C Henning, and R Orglmeister. The principles of software qrs detection. *IEEE Eng Med Biol Mag*, 21:42–57, 2002.

[29] H. Luepschen, S Leonhardt, and C. Putensen. *Yearbook of Intensive Care and Emergency Medicine.* Springer-Verlag Berlin Heidelberg, Germany, 2010.

[30] National Heart Lung and Blood Institute. Coronary angiography. `http://www.nhlbi.nih.gov/health/dci/Diseases/ca/ca_all.html`.

[31] National Heart Lung and Blood Institute. Coronary artery disease. `http://www.nhlbi.nih.gov/health/dci/Diseases/Cad/CAD_WhatIs.html`.

[32] Erik HW Meijering, Karel J Zuiderveld, and Max A Viergever. Image registration for digital subtraction angiography. *International Journal of Computer Vision*, 31(2/3):227–246, 1999.

[33] Committee on the Mathematics and Physics of Emerging Dynamic Biomedical Imaging. *Mathematics and Physics of Emerging Biomedical Imaging.* National Academic Press, Washington, D.C., 1996.

[34] Adel S. Sedra and Kenneth C. Smith. *Microelectronic Circuits.* Oxford University Press, 198 Madison Avenue,New York, New York, 1998.

[35] D. Spiegelhalter, J. Myles, D. Jones, and K. Abrams. An introduction to bayesian methods in health technology assessment. *British Medical Journal*, 319:508–512, 1999.

[36] Ambulance Technician Study. Cardiac. `http://www.ambulancetechnicianstudy.co.uk/card.html`.

[37] Pico Technology. Application for pico products: Electrocardiogram (ecg) project for drdaq. `http://www.picotech.com/applications/ecg.html`.

[38] Pico Technology. Picoscope 2000 series entry level oscilloscopes. `http://www.picotech.com/picoscope2000.html`.

[39] Wikipedia. File:64 slice scanner.jpg. `http://en.wikipedia.org/wiki/File:64_slice_scanner.JPG`.

[40] Wikipedia. File:ct-internals.jpg. `http://en.wikipedia.org/wiki/File:Ct-internals.jpg`.

[41] Wikipedia. Maximum a posteriori estimation. `http://en.wikipedia.org/wiki/Maximum_a_posteriori_estimation`.

[42] Wikipedia. Nyquistshannon sampling theorem. `http://en.wikipedia.org/wiki/Nyquist-Shannon_sampling_theorem`.